Revision 1

Mineralogy and geochemistry of hot spring deposits at Námafjall, Iceland: Analog for sulfate soils at Gusev crater, Mars

Word count: 11,623

George L. Carson[1,+]
Lindsay J. McHenry[1,*]
Brian M. Hynek[2]
Barry I. Cameron[1]
Chase T. Glenister[1]

* corresponding author

1. Department of Geosciences, University of Wisconsin- Milwaukee. 3209 N. Maryland Ave., Milwaukee, WI 53211. lmchenry@uwm.edu. Phone: 414 229-3951. Fax: 414 229-5452.
2. Laboratory for Atmospheric and Space Physics, University of Colorado Boulder, 1234 Innovation Drive, Boulder, CO 80303
+ Present address: 610 Winona Ct APT 28, Denver, CO 80204

Key words: Hydrothermal alteration; Mars analog; sulfate mineralogy

Abstract

Iceland's Námafjall geothermal area exhibits a range of alteration environments. Geochemical and mineralogical analyses of fumaroles and hot springs interacting with Holocene basaltic lavas at Hverir, and with Pleistocene hyaloclastites atop nearby Námaskar∂ hill, reveal different patterns of alteration depending on water-rock ratio, degree of oxidation, and substrate composition and age. The focus of this study is on the mineral deposits at and near hot springs at Hverir and Námaskar∂. Surface samples, and samples collected from shallow pits in the alteration aprons adjacent to hot springs, were analyzed by X-ray Diffraction (XRD) and X-ray Fluorescence (XRF) to constrain the differences in composition with both distance and depth. Fluids were analyzed in the field for their environmental parameters and sampled for cation and anion analysis. Fluid analyses revealed uniformly acidic conditions but with site-to-site variation in other parameters such as temperature, salinity, and conductivity. Solid phases identified include amorphous silica, pyrite, elemental sulfur, and kaolinite in the muds, surrounded by Fe^{2+}-sulfate and then Fe^{3+}- sulfate efflorescences, following a redox gradient pattern involving the oxidation of sulfur and then iron with increasing distance. Shallow pits excavated near two Námaskar∂ hot springs reveal a shallow oxidation front, with sulfide-rich materials below a thin surface of sulfates and elemental sulfur. Silica phases include amorphous silica and quartz. Quartz likely reflects diagenetic maturation of earlier-formed amorphous silica, under surface hydrothermal conditions.

The high iron content of the substrate basalt and the prevalence of Fe-sulfates and Fe-oxides among the alteration products makes this geothermal area an especially useful analog for potential Martian hydrothermal environments. In particular, these sulfate-rich deposits adjacent to volcanic, acidic hot springs could provide a helpful comparison for sulfur-rich soils in the Columbia Hills on Mars, where some of the same minerals have been identified (e.g. ferricopiapite) or inferred (e.g. rhomboclase).

Introduction

Volcanic hydrothermal deposits are key targets for astrobiological research, since they can provide warm, wet environments on or below otherwise inhospitably cold planetary surfaces, and since terrestrial examples provide a habitat for a variety of extremophile microorganisms. The characterization of likely hydrothermal deposits in the Columbia Hills explored by the Mars Exploration Rover (MER) Spirit (e.g., Yen et al., 2008), and the detection of likely hydrothermal deposits from orbit by the Mars Reconnaissance Orbiter (MRO, e.g. Skok et al., 2010), have made understanding the astrobiological potential of these environments a priority for NASA's Mars exploration program.

Iceland provides an excellent analog for potential Martian hydrothermal sites, because of its wide variety of hydrothermal environments coupled with their interaction with high-iron basalts comparable to those found on Mars. This study describes an analog site in northeastern Iceland (Námafjall), where acid-sulfate fumaroles and more reducing acidic mudpots and hot springs interact with relatively young basaltic lavas and hyaloclastites, forming alteration and precipitated products representing a range of temperature and redox conditions. The redox gradients observed in these deposits could provide an energy source for iron or sulfur reducing or oxidizing microbes.

The objectives of this work were to (1) characterize the mineral assemblages and major element distribution for altered and precipitated samples at the surface and at shallow depth at increasing distances from active hot springs at Námafjall, (2) conceptually model the processes of leaching and mineral precipitation in terms of changing pH, oxidation, and temperature conditions, and (3) consider these trends in the context of Mars hydrothermal deposits.

Background

Mars Hydrothermal Activity

Hydrothermal environments once occurred on the Martian surface, based on its long history of volcanic activity and evidence for past water. Such environments could have been habitable, providing heat, energy, and water for life even after the overall Martian surface conditions would have been too cold and dry (Walter & Des Marais, 1993; Schulze-Makuch et al., 2007; Hynek et al., 2013, 2018). Deposits from multiple landing sites have been interpreted as potentially hydrothermal, including Jezero crater carbonates (based on orbital spectroscopy, Tarnas et al., 2021), Gale crater tridymite (investigated by Curiosity, Yen et al., 2021), Meridiani Planum sulfate and hematite rich deposits (investigated by the Mars Exploration Rover (MER) Opportunity, McCollom and Hynek, 2005), and most notably multiple rocks and soils of the Columbia Hills at Gusev crater studied by MER Spirit.

Past hydrothermal activity in the Columbia Hills is indicated by evidence for hydrovolcanism (Home Plate, Squyres et al., 2007) and various mineralogical and geochemical trends in both outcrop and soil deposits. Silica-rich, opal-A bearing outcrops have been interpreted as near-neutral hot spring deposited sinters (Ruff et al., 2011, 2020; Ruff and Farmer, 2016), while silica-rich (e.g. Gertrude Weise class) and sulfate-rich (e.g. Paso Robles class) soils have been interpreted as acid-sulfate leached deposits formed in a fumarolic or hot spring environment (e.g.

Squyres et al., 2008; Morris et al., 2008). The Paso Robles class soils are sulfate-rich, with Ca, Mg, and ferric sulfates, along with amorphous silica and hematite; in the case of Paso Robles and Arad these have been interpreted as likely fumarolic deposits with lower water/rock ratios, while at the Tyrone locality conditions were likely wetter (Wang et al., 2008; Yen et al., 2008; Schmidt et al., 2008; 2009; Hausrath et al., 2013). Peace class rocks in the Columbia Hills are composed of mafic to ultramafic mineral grains cemented by sulfate salts, potentially derived from hydrothermal processes as well (e.g. Ming et al., 2006). Properly assessing the potential habitability of the altered soils will require reconciling these different interpretations.

Iceland

Iceland’s Northern Volcanic Zone, a product of the Mid-Atlantic Ridge and the Icelandic mantle plume, hosts the Krafla central volcano. Subglacial eruptions during the Pleistocene produced basaltic hyaloclastites, while subsequent eruptions in the Holocene have emplaced subaerial lavas at various intervals ranging from 250- 1000 yrs. This work will focus on the Namafjall area where intense surface hydrothermal alteration is currently affecting the subglacial Pleistocene hyaloclastites and the postglacial Holocene lava flows.

The Krafla volcano hosts the Namafjall geothermal field on its southern edge, where hydrothermal fluids travel along fault planes to the surface (Figure 1). The basaltic hyaloclastite atop and along the margins of the Námaskar∂ hyaloclastite ridge interacts with rising hydrothermal fluids, as do Holocene basaltic lava flows at Hverir at the base of the ridge. Subvertical gypsum veins crosscut the hydrothermally-altered hyaloclastites, and are related to the faulting and fissures of the Krafla fissure swarm (Figure 1a). Talus deposits on Námaskar∂ are composed of clay blocks, clayey siltstones, and gravelly conglomerate lenses and beds (Geptner et al., 2007). East of Námaskar∂ lies the Hverir geothermal field, which hosts a cluster of fault-related fumaroles along with hot springs and mudpots (Saemundsson et al., 2012). Surface materials transported from local drainages including the nearby Námaskar∂ ridge interact with these hydrothermal features. The Late Holocene lava field immediately east of the geothermal field contains large circular fumarolic aprons up to ~25 m wide that currently produce little to no volcanic emissions; these are described in detail in Carson et al. (in review). The current study focuses on the hot springs and mudpots of both Hverir and Námaskar∂.

Methods

Site details

Hverir: hot spring transect. In the central Hverir hot spring and mudpot field (Figure 2c), we selected one hot spring (shown in Figure 2a) and collected muddy water, mud from the edge of the pool, and surface mineral crusts within about two meters, targeting changes in color (from white to orange). Temperature, distance from the pool's edge, and appearance are reported for each sample. Samples and water measurements were collected in 2013, 2014, 2016, and 2017. The "substrate" for this site is difficult to assess, as the area likely receives some sediment from both the Holocene basaltic lava directly to the east (sample IV-13-15) and the Pleistocene Námaskar∂ hyaloclastite ridge to the west (sample IV-14-36).

Námaskar∂: hot spring depth profile. At the top of Námaskar∂ hill, we selected two hot springs and their surrounding alteration aprons and collected fluid, mud from the edge of the pool, surface mineral crusts, and excavated a shallow pit within the apron to collect samples from depth (Figures 4 and 5). We targeted changes in color and appearance (darker grey at depth). Temperature, distance from the pool edge, and depth (if appropriate) are reported for each sample. Samples and water measurements were collected in 2014, 2016, and 2017.

Sampling Protocols

All samples analyzed in this study are summarized in Tables 1 (Hverir hot spring transect) and 2 (Námaskar∂ hot spring transects). Precipitate samples were collected by carefully scraping surface materials over a small area into a plastic sample bag, and altered soils were scooped using a spatula. Fluid samples were scooped using a plastic bottle that had been pre-contaminated with the fluid being sampled, attached to the end of a Jacob's staff. Temperatures were measured for each sample using a thermometer, and pH of fluid was estimated using overlapping pH papers. Less altered "substrate" samples were collected away from the thermal features along the Námaskar∂ hyaloclastite ridge (IV-14-36) and from the Holocene basaltic lava flow at the eastern margin of Hverir (IV-13-15).

For select fluid samples, an HL4 Hydrolab sonde was used in the field to measure pH, temperature (T), conductivity, oxidation/reduction potential (ORP), dissolved oxygen, salinity, and total dissolved solids (TDS). For fluids cooler than 50°C, the Hydrolab sonde was deployed directly, for hotter fluids, a sample was allowed to cool in a full, covered container until it was below 50° C and then analyzed. Collected fluid samples were filtered into two 60 mL bottles through a 0.2 micrometer cellulose filter. One bottle of sampled fluid (for cations) was acidified (using 4N nitric acid) for samples with pH above 3, for more acidic samples, one sample was collected for both cations and anions.

Laboratory Analyses

Samples were air dried and ground using a Rocklabs Shatterbox for competent samples (basalts) and an agate mortar and pestle without the addition of liquids. X-ray Diffraction (XRD) was completed and analyzed at UW Milwaukee (UWM) using a Bruker D8 Focus XRD (Cu tube, 0.02° 2 Theta step size, 2–60° 2 Theta, 1 s/step, scintillation detector: see McHenry et al., 2017). Phases were identified using Bruker's EVA software and the International Centre for Diffraction Data Powder Diffraction Files (ICDD PDF) 2 database for comparison. Phases were characterized as major, minor, or absent based on a qualitative assessment of relative peak heights.

Samples that were determined not to be dominated by sulfur-bearing phases based on XRD were further prepared for X-ray Fluorescence (XRF) analysis. Powdered samples were dried overnight at 105°C. A split of each dried sample was analyzed for loss on ignition (LOI) using a muffle furnace. Another split (1.0000 g, ± 0.0003 g) of the same dried powdered sample was then mixed with 10.0000 g (± 0.0003 g) of a 50/50 Lithium Metaborate/ Lithium Tetraborate flux with an integrated LiBr non-wetting agent and ~1 g of ammonium nitrate (oxidizer) in a platinum crucible and fused into a glass bead using a Claisse M4 fluxer. Beads were then analyzed for major and minor elements using a Bruker S4 Pioneer XRF, following methods of Byers et al. (2016). Eleven USGS rock standards were used to construct a calibration curve from which concentrations were calculated. Since sulfur is partially lost during the fusion process, select samples for which sufficient material was available were also prepared as pressed pellets. 7.5 grams of dried, powdered sample was combined with three GeoQuant wax binder pellets (0.94 g total) in a shatterbox, and then pressed at 25 tons for one minute in an Atlas T25 semiautomatic press. Pellets were then analyzed by XRF with concentrations determined using a calibration curve based on six USGS rock standards (methods described in Byers et al., 2016). Only sulfur is reported from the pressed pellets, as the fused bead calibration is better for all other elements.

Five fluid samples were analyzed for major cations using a Thermo iCE 3000 Series Atomic Adsorption Spectrometer using SOLAAR Series software. Major anions were analyzed using a single column Dionex ICS 1000 Ion Chromatograph with an AERS 500 Suppressor using a 4.5mM Na_2CO_3/1.4mM $NaHCO_3$ buffer solution. Silica was analyzed using a SEAL Analytical AA3 HR auto analyzer. Quantitative analysis was accomplished using a calibration curve from stock standards of each element provided by the UWM School of Freshwater Sciences. For most samples, dilution was needed to fit the calibration curve. An electrical balance was calculated to determine the accuracy of analysis. Many samples had a significant electrical imbalance, which is assumed to be attributed to high Al concentrations (not analyzed) based on published results for another Icelandic hydrothermal system (Kaasalainen & Stefánsson, 2012). Aluminum is difficult to calibrate in solution due to its relative insolubility under near-neutral pH conditions.

Inferred aqueous Al concentrations were calculated by charge balancing fluid samples to <5 %. Several samples were already charge balanced and thus do not include Al concentrations.

Results

XRD results

XRD results (Tables 1-2) reveal diverse mineral assemblages that vary depending on the specific environment. Sulfur-bearing minerals are abundant and include sulfides (pyrite, marcasite), elemental sulfur, and a wide range of sulfates:

Ca: gypsum
Al: alunogen ($Al_2(SO_4)_3 \bullet 17H_2O)$)
Fe^{3+}: rhomboclase ($(H_5O_2)^+Fe^{3+}(SO_4)_2 \bullet 2H_2O$)
ferricopiapite ($Fe^{3+}_{2/3}Fe^{3+}_4(SO_4)_6(OH)_2 \bullet 20H_2O)$)
Fe^{2+}: rozenite ($Fe^{2+}SO_4 \bullet 4H_2O$)
szomolnokite ($Fe^{2+}SO_4 \bullet H_2O$)
mixed cation: pickeringite ($MgAl_2(SO_4)_4 \bullet 22H_2O$)
halotrichite ($Fe^{2+}Al_2(SO_4)_4 \bullet 22H_2O$)
natroalunite ($NaAl_3(SO_4)_2(OH)_6$)
jarosite ($KFe^{3+}(SO_4)_2(OH)_6$),
voltaite ($K_2Fe^{2+}_5Fe^{3+}_3Al(SO_4)_{12} \bullet 18H_2O$)
coquimbite ($AlFe^{3+}_3(SO_4)_6(H_2O)_{12} \bullet 6H_2O$
tamarugite ($NaAl(SO_4)_2 \bullet 6H_2O)$)

Other phases include silica phases (amorphous silica, cristobalite, and quartz), oxides (anatase and goethite), and clay minerals (smectite and kaolinite). As the clay size fraction was not separated for analysis, our characterization of the clay phases is limited to distinguishing between "smectite" (clays with first-order basal spacing around 14 angstroms, based on XRD) and kaolinite.

Figures 3-5 show representative XRD patterns for samples from the vicinity of hot springs at Hverir (Figure 3) and Námaskar∂ hill (Figures 4 and 5). Hot spring acid-sulfate alteration produced three distinct mineral assemblages: (i) gray sediment that includes pyrite/marcasite + anatase ± amorphous silica ± kaolinite ± elemental sulfur, (ii) white surface precipitates that include halotrichite group + gypsum ± Fe^{2+} sulfates ± Fe^{3+} sulfates, and (iii) orange precipitates and underlying sediment that include smectite + Fe^{3+} sulfates + amorphous silica ± anatase ± goethite. Differences between surface and deeper samples are visible in both the appearance and mineral assemblages observed, with the pyrite-bearing grey mud observed both in the hot springs and at depth in shallow pits. Pyrite is absent from surface and shallow samples at the site of the pits away from the edge of the hot springs, which are instead dominated by elemental sulfur and various sulfate minerals.

XRF results

Altered rocks and soils in the vicinity of hot springs show a range of elemental compositions (OM Tables 3-4), reflecting their formation environments and mineral assemblages. Heavily leached samples show elevated SiO_2 and TiO_2 concentrations (up to 76.4 and 10.7 wt%, respectively), while pyrite-rich muds are elevated in Fe_2O_3 (up to 28 wt%) (Figure 6). Less altered hyaloclastite (sample IV-14-36, collected away from thermal features) reveals a basaltic "substrate" composition with 49.3 wt% SiO_2 and relatively high iron (14.1 wt% Fe_2O_3T). TiO_2 for the substrate sample was 2.19 wt%, lower than the TiO_2 observed in most of the altered samples from Námaskar∂ hill. The composition of the Hverir lava substrate sample (IV-13-15) is similar, with 48.8 wt% SiO_2, 15.4 wt% Fe_2O_3T, and 1.82 wt% TiO_2. Sulfur was only analyzed for a subset of samples, but where analyzed shows enrichment in altered samples (3.4-20 wt% SO_4) compared to the substrate (0.18 wt% SO_4 for Námaskar∂ hyaloclastite, 0.11 wt% for Hverir basalt). Most cations (Al, Na, K, Ca, Mg, Mn) are lower in the altered rocks and soils than in the substrate. These trends are shown in spider plots, in which the compositions of altered samples are plotted against the less altered substrate (Figure 7). Iron (reported at Fe_2O_3T) is variable throughout the study area, as reflected by the colors observed during sampling.

Fluid results

Results of the field Hydrolab analyses are reported in Table 5. For fluids analyzed at Hverir and Námaskar∂, pH varies over a narrow range (2.15-2.42). All sites are at least mildly reducing (negative oxidation-reduction potential (ORP)), but salinity, conductivity, and total dissolved solids (TDS) vary from site to site. While the highest salinity (3.41 ppt) and TDS (4.0 g/l) are recorded in Hverir sample IV-14-1, Námaskar∂ sample IV-14-23 also has high values (2.32 ppt and 2.7 g/l). The lowest salinity (0.77 ppt) and TDS (0.9 g/l) measured were for Námaskar∂ sample IV-14-29, though Hverir sample IV-14-4 also has low values (1.13 ppt and 1.3 g/l). Results of the chemical analysis of anions and cations are reported in Table 6. The samples with the highest salinities (based on the Hydrolab results) also contain the highest concentrations of SO_4^{2-} and Mg^+ (up to 3819 mg/l and 82.4 mg/l, respectively, for sample IV-14-01), while all dissolved ions had low concentrations for the least saline sample (IV-14-29). Regardless of salinity, the Námaskar∂ samples have lower concentrations of Na^+ and K^+ than do samples from the Hverir fluids.

Discussion

Distribution of phases, based on environment

In the vicinity of the hot springs, conditions were reducing near the source and at depth and more oxidizing at the surface and further away, based on the mineral assemblages observed. The mud at the margin of a hot spring in Hverir (sample IV-13-2) contained both elemental sulfur and pyrite, along with kaolinite. Precipitates at increasing distance from this feature contain abundant sulfates, including pickeringite or halotrichite and gypsum nearby (sample IV-13-3), with rhomboclase further away (sample IV-13-4). This reveals a trend in redox conditions, with reduced sulfur and iron at the source, more oxidized sulfur (as sulfate) and reduced iron (Fe^{2+}) nearby, and sulfate and oxidized iron (Fe^{3+}) at greater distances.

The two sampling sites at and near hot springs on the top of Námaskar∂ hill demonstrate a range of reducing and oxidizing conditions. At the first spring, amorphous silica and anatase are present in all samples (IV-14-30, 31, and 32), a result of acid leaching and associated residual enrichment of silica and titanium. The surface at the top of the pit (sample IV-14-31) reflects oxidizing conditions, with the Fe^{3+} sulfate mineral rhomboclase and only minor elemental sulfur. At shallow depth (sample IV-14-32), elemental sulfur is more abundant and ferricopiapite appears. At depth (sample IV-14-30), pyrite and marcasite are the dominant sulfur-bearing phases. This reflects a trend towards more reducing conditions at depth. Based on the position of the color change between the lighter grey (elemental sulfur rich) and darker grey (sulfide rich) layers, this oxidation front appears to occur at about 10 cm depth.

A second pit near another hot spring on Námaskar∂ reveals a similar pattern, with Fe^{3+} sulfate minerals (ferricopiapite and jarosite) at the surface (sample IV-14-24), leached material slightly below the surface (sample IV-14-25: anatase, minor amorphous silica, and quartz), and pyrite together with Fe^{2+} sulfate minerals (szomolnokite and rozenite) at shallow (8 cm) depth (sample IV-14-26). The presence of quartz rather than amorphous silica at this site suggests a higher degree of diagenetic maturation. Since the substrate is basaltic hyaloclastite and the site is on the top of a ridge, the quartz must be related to the local hydrothermal environment (either past or present). A white surface efflorescence at this site (sample IV-14-22) consists entirely of precipitated sulfate minerals, almost entirely from the halotrichite/pickeringite group, with minor gypsum and tamarugite identified. While halotrichite and pickeringite are difficult to distinguish using XRD alone, all or most of this sample is likely halotrichite. This is because of the high background when analyzed by XRD using a scintillation detector (consistent with Fe fluorescence), a qualitatively better pattern match with halotrichite, and the overall abundance of Fe-S phases in all samples from this locality.

A study by Black et al. (in revision) explored a set of different (but complimentary) hot springs at Námaskar∂, and applied VNIR analyses to collected samples. The VNIR analyses they report help resolve some of the questions about specific minerals that are difficult to detect or distinguish using XRD alone. In particular, their VNIR analyses confirm the presence of pickeringite (rather than halotrichite) in a hot spring transect sample that also bears voltaite and identifies the clay mineral nontronite in the apron of a fumarole.

While the current study at Námaskar∂ focuses on deposits in the vicinity of hot springs, El Maarry et al. (2017) examined two transects near Námaskar∂ fumaroles nearby. They report mineral assemblages with elemental sulfur near the source (rather than sulfide minerals), amorphous silica and anatase nearby, and alunite and hematite (along with amorphous silica) further out. This indicates more oxidizing conditions associated with fumaroles compared to hot springs in the same hydrothermal field. Carson et al. (in review) also found mineral assemblages consistent with more oxidizing conditions (sulfates but no sulfides) surrounding a fumarole in Hverir, to the east of the hot springs sampled for the current study.

Element Mobility

Comparing the elemental conditions of sediment samples near the hot springs to the less altered hyaloclastite composition (IV-14-36) shows how these sediments differ from their substrate. Figure 7 shows a spider plot of six altered samples, plotted against the hyaloclastite. All samples show similar element enrichment and depletion patterns. Silica is enriched in three samples (IV-14-25, IV-14-31, and IV-14-32), and elevated TiO_2 and Zr in most samples (Figure 6) indicate significant residual enrichment via acid-sulfate leaching. Note that silica is not enriched in all samples that contain elevated TiO_2 and Zr concentrations. Ti and Zr appear to be a stronger indicator of leaching and resulting residual enrichment than silica and are concentrated in samples that have undergone significant clay development as well as those dominated by amorphous silica.

Mg, Ca, Na, and K are depleted in all samples analyzed by XRF, and iron is significantly depleted in some (Figure 7). Those with enriched iron (up to 28.09 wt% Fe_2O_3T) typically contain abundant pyrite in their XRD patterns, and lower SiO_2 and higher Al_2O_3 concentrations (Figure 6). The depletion of Ca, and lack of Ca-sulfate minerals, is unusual for this kind of environment. Ca could have been locally mobilized and reprecipitated in the abundant veins of gypsum observed cross-cutting Námaskar∂ hill.

Aqueous Geochemistry

The composition of selected geothermal surface waters at Námafjall are provided in Table 6, and their associated environmental parameters are reported in Table 5. Five fluid samples (listed in Tables 1 and 2, photographs of sample sites in Figures 2, 4, and 5) from geothermal features (e.g. acid pools, hot springs, drainage channels, etc.) in the Hverir and Námaskar∂ area were analyzed. The sampled fluids had temperatures between 11-71°C and pH within a narrow range (2.15-2.42), consistent with their steam-derived acid-sulfate origin. Acidity is controlled by the oxidation of H_2S to sulfate, resulting in a decrease in pH values. The oxidation of dissolved sulfide proceeds slowly through SO_3^{2-} and $S_2O_3^{2-}$ and eventually to sulfate. Intermediate oxidation states are unstable in acidic waters and rapidly oxidize in the presence of pyrite, which is a common phase in acid pools and hot springs (Kaasalainen & Stefánsson, 2011) and which is observed in our study in and near hot springs at Hverir and Námaskar∂. Additional acid is generated by the oxidation of elemental sulfur in the following reaction:

$$S^0 + 1.5O_2 + H_2O \rightarrow 2H^+ + SO_4^{2-}$$

A floating film of pyrite and elemental sulfur was commonly associated with acid sulfate pools and hot springs, suggesting that dissolved sulfur was lost to the formation of sulfur-bearing minerals. H^+ concentrations are typically higher than transition metal cations in solution, and rock dissolution buffered the pH by consuming protons during water-rock interactions. This process is analogous to an acid-base titration, where H^+ ions are consumed by the basalt, which subsequently releases cations into solution. The pH is also buffered by the second dissociation constant of sulfuric acid (HSO_4^-/SO_4^{2-}) (Kaasalainen & Stefánsson, 2012).

Geothermal fluid compositions exhibit significant variability but, in general, major cations showed a decrease in abundance in the following order: SiO_2, Fe^{2+}, Al^{3+}, Ca^{2+} or Mg^{2+}, Na^+, K^+, although the inferred Al^{3+} concentration varied substantially between water samples. The inferred elevated Al^{3+} concentrations correspond to the highest sulfate concentrations in hot springs (up to 450 mg/l) and are reasonable based on results of previous and similar studies (up to ~1100 mg/l) (Kaasalainen & Stefánsson, 2012).

Acid-sulfate waters are dominated by sulfate anions, ranging from 398 to 3819 mg/l. The highest sulfate concentrations (~3800 mg/l) were found in the Hverir hot springs, though concentrations of 2150 mg/l were observed for one sample from the top of Námaskar∂ hill. Differences in dissolved sulfate concentrations may be the result of the differences in gas chemistry between the two geothermal areas (e.g. Ármannsson, 1993). Additionally, it may be a function of the discharge intensity, where higher discharge rates transport more dissolved species in solution to the surface, rather than diffusing out into the altered deposits. Chlorine is depleted (<2 mg/l) compared to local source water due to its high mobility during the alteration process and steam condensate dilution (Arnórsson and Andrésdóttir, 1995, Kaasalainen and Stefánsson, 2012). Nitrate is found in minor concentrations (<9 mg/l).

Iron-Sulfide Formation and Oxidation

The Fe-sulfide minerals pyrite and marcasite were observed near hot springs at Hverir and atop Námaskar∂ hill. A high supply of H_2S gas produced a locally reducing environment with high water-rock ratios, where the oxidation front extends all the way to the surface. In areas with lower temperature and H_2S supply, pyrite is found at depth below the oxidation front.

The oxidation of pyrite is a complex biogeochemical process involving hydration, hydrolysis, redox reactions, and microbial catalysis in the reaction below:

$$FeS_2\ (aq) + 3.75O_2\ (g) + 3.5H_2O\ (l) \rightarrow Fe(OH)_3(s) + 2H_2SO_4(aq)$$

The rate of pyrite oxidation depends on a variety of factors that include T, pH, Eh, relative humidity, surface area, and microbial action. Ultimately, the driving force for the breakdown of pyrite and marcasite is interaction with H_2O and atmospheric O_2. This results in the oxidation of more soluble Fe^{2+} to insoluble Fe^{3+}, often in the form of goethite or eventually hematite, and the formation of sulfuric acid (Markússon and Stefánsson, 2011). Acidic hydrothermal solutions precipitate efflorescences of soluble and insoluble sulfate-salts. The former, although ephemeral, provide direct evidence for the pathways of sulfide oxidation and the alteration of associated mineral assemblages. Adjacent to the Námaskar∂ and Hverir hot springs, a shallow oxidation front (with sulfides below and sulfates above) forms where the hydrothermally-precipitated pyrite and marcasite alters in contact with surface conditions. Thermophilic Fe- and S-chemoautotrophs can also play an important role during the oxidation of pyrite, though Ende and Szynkiewicz (2022) found little evidence for microbial activity in these kinds of acidic hot springs, likely due to the elevated temperature.

Efflorescence of Soluble Sulfate-Salts

Bulbous and fibrous aggregates formed white surface efflorescences around the hot springs. Hot and acidic conditions dissolve primary igneous phases and mobilize Fe^{2+}, Al^{3+} and other mobile cations out of the system. Previous studies (e.g. Zolotov and Shock, 2005) indicate that sulfide reacts more quickly than Fe during pyrite oxidation, giving rise to aqueous solutions enriched in SO_4^{2-}, H^+, and Fe^{2+}.

The oxidation of Fe-sulfides and supply of mobile cations allowed for the precipitation of a variety of Fe^{2+}-, Fe^{3+}-, Al-, Ca-, and Mg-insoluble and soluble sulfate-salts. Acidic hot springs had high SO_4, Fe, and Al aqueous concentrations, and at both Hverir (IV-13-3) and Námaskar∂ (IV-17-7) a widespread zone of halotrichite and/or pickeringite ($(Fe^{2+},Mg)Al_2(SO_4)_4 \bullet 22H_2O$) surface precipitation is observed. Extensive solid solution occurs in these minerals, where Fe>Mg the mineral is classified as halotrichite, and pickeringite is more magnesium-rich. Their XRD patterns are very difficult to distinguish and, therefore, a positive identification of either mineral is labeled as halotrichite/pickeringite. Bilinite ($Fe^{2+}Fe^{3+}{}_2(SO_4)_4 \bullet 22H_2O$) also forms a solid solution series with halotrichite (identified by Geptner et al., 2007), indicating additional solid solution between mixed valence states of Fe, and apjohnite ($Mn^{2+}Al_2(SO_4)_4 \bullet 22H_2O$) is also very similar in its XRD pattern. For sample IV-13-3 (Hverir hot spring transect) some of the halotrichite/pickeringite is likely pickeringite, as the sample has 2.15 wt% MgO as measured by XRF and pickeringite is the only Mg-bearing phase identified by XRD. For sample IV-14-22 (Námaskar∂ hill), halotrichite is more likely, given elevated XRD background and a qualitatively better pattern match with halotrichite. Black et al. (in revision) confirmed the presence of pickeringite (rather than halotrichite) in a sample from the margins of a different Námafjall-area hot spring using VNIR (along with voltaite in the same sample, identified using XRD), though they also observed abundant halotrichite/apjohnite in a sample from a fumarole transect. A variety of minerals from the halotrichite group thus appear to be present at Námafjall.

Ferrous iron sulfates (rozenite, halotrichite, and szomolnokite) were found in the white to orange surface precipitate samples IV-13-3 (Hverir hot spring transect) and IV-17-7 (Námaskar∂), though IV-13-3 also contained minor mixed valence (voltaite) and ferric iron sulfate (coquimbite, rhomboclase) as well. Previous investigations of sulfate-salts in volcanic and acid-mine drainage environments reveal that the formation of rozenite comes first and through a slow recrystallization process forms szomolnokite (Reardon & Beckie, 1987).

Alunite-jarosite group minerals are observed in both field areas, though only as minor phases. Natroalunite is found in sediment samples from the upper cm of the first Námaskar∂ sample pit, in samples otherwise dominated by amorphous silica, anatase, and elemental sulfur. It is identified as a minor phase in the mud at the edge of the sampled Hverir hot spring, along with pyrite, elemental sulfur, and other sulfate phases (including jarosite), showing a range of redox conditions in the same sample.

Phyllosilicates

Kaolin and smectite group minerals are the main phyllosilicates at Námafjall. The two mud samples collected from the edge of hot springs (IV-13-2 from Hverir, IV-17-05 from the second sampled hot spring at Námaskar∂) both yielded kaolinite, as did the sediment at the base of the pit excavated near the first Námaskar∂ hot spring (IV-14-30). All three kaolinite-bearing samples also contained pyrite and anatase. Kaolinite crystallinity improves in low pH environments, though kaolin group minerals are more stable in mildly acidic to neutral environments (Fialips et al., 2000).

Smectite is a major phase in two samples analyzed, both from orange surface sediment samples (at Hverir: IV-13-4; at Námaskar∂: IV-14-24). Both samples also contain amorphous silica and abundant sulfate minerals. In general, smectite is more abundant in areas with lower temperatures and lower gas emissions, where the neutralization of acidic fluids thermodynamically favors smectite formation. Mínguez et al. (2011) observed a range of smectite compositions that reflected the composition of the Holocene basalts and Pleistocene hyaloclastites at Námafjall. For example, Al-rich smectite (beidellite and montmorillonite) was more abundant in the hyaloclastite, while nontronite (Fe^{3+}-bearing smectite) was more abundant associated with altered basalt. However, Black et al. (in revision), in a study of the mineralogy surrounding a Námaskar∂ hill fumarole, identified nontronite (using VNIR) at the outskirts of an alteration apron, where the substrate was hyaloclastite. The varying compositions may also reflect changes in the acidity of the fluids, where the extent of alteration affects the amount of cations released into solution. Additionally, increased distance from the pathway of hydrothermal fluids will raise the pH and neutralize the acidity within the system and, thereby, precipitate out minerals containing more mobile elements (e.g. Ca, Mg). The composition of smectite depends on a combination of several factors including the pH of the fluid, element mobility, and the pathway of the fluids.

It is important to remember that the genesis of poorly crystalline smectite clays comes from the hydration of sideromelane fragments, i.e. palagonite. Through continued alteration, palagonite transforms into smectite, hence, smectite is an abundant mineral phase in areas of lower surface activity (in terms of temperature and gas emissions) along hyaloclastite ridges.

Thermodynamic models indicate that phyllosilicate formation is favored by moderate to alkaline pH conditions (e.g. Velde, 1995). However, kaolinite can precipitate under lower pH conditions

(Fialips et al., 2000). The stability of phyllosilicates in low pH systems with high ionic strength is not well constrained. For example, Al-phyllosilicates are less susceptible to alteration under acidic conditions than Mg-smectites such as saponite. However, Story et al. (2010) indicate that Al- and Fe/Mg-phyllosilicates can persist in sediments submerged in acid-saline lakes in Western Australia. In addition, Peretyazhko et al. (2014) was able to artificially form saponite and nontronite from reactions with basaltic glass under moderately acidic (pH 4) conditions. Also, Hynek et al. (2013) documented kaolinite in altered basalts in and around acid-sulfate fumaroles and hot springs with pH as low as 2 and montmorillonite at pH 4 at Cerro Negro volcano, Nicaragua. One important observation is the co-occurrence of smectite and jarosite in medium to low activity areas (sample IV-14-24), suggesting that smectite may be able to form *in-situ* under mildly acidic conditions in the presence of high ionic strength solutions. This observation indicates that smectite can persist and remain stable near low pH local discharge areas.

Silica and anatase

Many samples collected near the hot springs display a significant amorphous silica “hump” in their XRD patterns. One sample (IV-13-4 from the Hverir hot spring apron) contains minor cristobalite as well. Quartz was observed in two samples collected at depth from the second pit at Námaskar∂ (samples IV-14-25 and 26).

Samples with abundant amorphous silica are almost always also associated with anatase and elevated concentrations of both SiO_2 and TiO_2 measured by XRF, consistent with acid-sulfate leaching of the surrounding rocks and soils at low to moderate temperatures. Other elements are leached away, leaving a residual concentration of these less mobile elements. SiO_2 is initially housed in amorphous silica, while TiO_2 is housed within anatase.

Quartz and cristobalite are inferred to be secondary in nature, as the original substrate is Pleistocene basaltic subglacial hyaloclastite, and neither was identified (or expected) in the less altered hyaloclastite samples. While cristobalite and tridymite often occur as a high-temperature silica polymorph (if quenched rapidly from high temperatures, they can exist metastably at the surface), they can also form from the devitrification of volcanic glass (Heaney, 1994) and have also been identified as a likely fumarolic precipitate at Kilauea (Morris et al., 2000). The quartz in the Námaskar∂ samples most likely formed as the result of alteration or diagenesis either under the current hydrothermal regime, or at some earlier time since the Pleistocene emplacement of the hyaloclastite ridge. The formation of quartz due to the “maturation” of opal-A following hydrothermal sinter precipitation or acid-sulfate precipitation or leaching has been estimated to take thousands to tens of thousands of years (Herdianita et al., 2000; Rodgers et al., 2002, 2004), or as little as hundreds of years (Taupo volcanic area: Lynne et al., 2007) or even months (Lynne et al., 2006), depending on the specific conditions. Higher temperatures like those found in long-lived acid sulfate fumarolic systems help accelerate the process.

Anatase is observed in the XRD patterns of almost all amorphous silica or kaolinite-bearing samples and is a product of residual enrichment of immobile TiO_2 during leaching. While it is observed even for a sample in which TiO_2 is not significantly concentrated compared to the hyaloclastite substrate (substrate sample IV-13-15: 1.82 wt% TiO_2, minor anatase bearing Hverir sample IV-13-2: 2.56 wt% TiO_2), it is particularly abundant in samples from the vicinity of the

Námaskar∂ hot springs, which have higher TiO_2 concentrations (up to 10.7 wt% in sample IV-14-25).

Overall Water-Rock Interaction, Secondary Mineralogy, and Fluid Chemistry at the Surface

Hydrothermal surface alteration of Pleistocene hyaloclastites generates a mosaic distribution of varying surface colors and compositions along the margins of surface activity as the result of aggressive and changing geothermal conditions associated with the appearance and renewal of faults and fissures. The combination of element mobility and the formation and precipitation of hydrothermal assemblages has resulted in distinct mineralogical and geochemical trends in the alteration aprons around the hot springs. The supply of acid and volcanic gases (such as H_2S), the extent of the reaction, the pH of the water, and the position of the oxidation front (and related redox conditions) are the dominant processes within a volcanic geothermal system (Markússon and Stefánsson, 2011).

Acid-sulfate waters are produced when rising volcanic vapors are enriched in H_2S and CO_2, condensing into oxygenated ground- and surface-waters where the H_2S is oxidized into sulfuric acid and the CO_2 is mostly degassed (Kaasalainen & Stefánsson, 2012). This process produces acidic waters with pH <4 and reducing conditions that will alter the basaltic hyaloclastite and basalt lava flows in gas- (low water-rock ratios, fumaroles) and fluid- (high water-rock ratios, hydrothermal pools) dominated settings. Dissolved ion concentrations correspond well to bulk hyaloclastite and basalt compositions, indicating that the substrate dissolves nearly stoichiometrically (at pH <2.5) with respect to most major rock-forming elements. In acid-sulfate hydrothermal experiments on Central American basalts described by Marcucci and Hynek (2014), plagioclase dissolved first, followed by pyroxene and then olivine, with glass being the most resistant to dissolution (kinetically inhibited). Overall, dissolved ion concentrations are related to pH, with higher acidity associated with greater cation abundances.

These high-temperature and localized fluids become supersaturated with respect to pyrite, kaolinite, amorphous silica, and native sulfur (Markússon and Stefánsson, 2011). While amorphous silica, anatase, and kaolinite are insensitive to redox conditions, pyrite and native sulfur oxidize through interactions with atmospheric O_2 and H_2O, introducing more sulfuric acid into the system. Phase segregation and sulfur oxidation are the main controls on the pH of the fluid. In gas-dominated settings, secondary minerals can precipitate directly from the volcanic vapors or during alteration of primary igneous phases. In contrast, alteration products in fluid-dominated settings are controlled largely by the oxidation of iron sulfide deposits.

Hot Springs Alteration Model

A conceptual model of alteration for the hot springs is shown in Figure 8. The influx of H_2S gas results in extensive pyrite and native sulfur deposits, enriching alteration products in S (5.31-7.86 wt%). Acid leaching dominates closest to the hot spring, resulting in significant depletion of most major elements. This area also features a residual enrichment in SiO_2, TiO_2, and Zr, due to the removal of other components (as illustrated in X_2, Figure 9). In the orange sediments and precipitates along the margins, most elements are still depleted with the exception of phosphorous and iron (X_1, Figure 8). Fe and Al mobility are lower in these sediments as these elements are incorporated into clay minerals and Fe-bearing sulfates and sulfides. Iron and sulfur mineral assemblages depend largely on the position of the oxidation front, defined by the transition from reduced to oxidized mineral phases.

Pyrite oxidation generates a secondary mineral series associated with increasing distance from the hot spring in the following order: pyrite → rozenite → szomolnokite/ halotrichite group → jarosite → hematite/goethite (e.g. Nordstrom & Alpers, 1999). Fluid compositions near hot springs have enriched ferrous Fe concentrations (122-196 mg/l) that become supersaturated with respect to iron-sulfide minerals (Markússon and Stefánsson, 2011). Pyrite oxidation forms a series of soluble sulfate-salts, which likely reflects the lower mobility of Fe and S in the fluid phase due to increasing oxidation. Here, Fe- and S- redox gradients develop, and can be seen in the formation of sulfides under reducing conditions and the formation of sulfate-salts and oxides as they undergo varying degrees of oxidation.

Ultimately, the further from the discharge source the more control atmospheric O_2 exerts on the secondary mineral phases and element mobility. The predominance of Fe- and Al-sulfates reflects the dominance of these dissolved species in the fluids, while Ca^{2+} and Mg^{2+} are minor components in both the aqueous and mineral phases. Fe^{2+}-sulfates (e.g. white precipitates) are only observed in areas of high to medium surface activity (e.g., moderate to high temperatures and gas emissions). This suggests that these minerals may also be temperature dependent, or can be dissolved and transported during precipitation events in areas of lower activity.

At the surface, iron and sulfur oxidation occurs over several meters, while below the surface the oxidation front exhibits a sharp boundary over several centimeters (Figure 4). In two depth profiles, a thin laterally-continuous transitional layer (<5 cm) separates the oxidized from the reduced layer, but mineralogically is more similar to the oxidized surface layer. In low activity areas, pyrite appears to alter directly into goethite and/or hematite, rather than through a series of soluble sulfate-salts (Nordstrom & Alpers, 1999). Markússon and Stefánsson (2011) observed a similar trend at Krýsuvík, Iceland, where Cu-sulfide (covellite) was present below the oxidation front and Cu-sulfates at the surface. At Námafjall, Fe- sulfates (both Fe^{2+} and Fe^{3+}) dominate the sulfate mineralogy at the surface away from neighboring hot springs, and along the margins of activity, Fe^{3+} sulfates and even goethite indicate more oxidizing conditions. At Hverir, smectites are found along the distal margins of surface activity, where the neutralization of the acid-sulfate fluids favors smectite formation.

Ende and Szynkiewicz (2022), in their studies of fluid chemistry of varied terrestrial hot spring environments (including Námafjall), concluded that the oxidation of Fe^{2+} to Fe^{3+} is more efficient during drier (fumarolic) intervals compared to wetter (hot spring) intervals in the same hydrothermal H_2S-emitting settings. This is consistent with our observation of Fe^{2+} sulfides and sulfates in hot spring muds and directly adjacent altered sediments and Fe^{3+} sulfates in surface deposits further from the fluid source.

Relevance to Martian Hydrothermal Systems

While Iceland in general and the Námafjall geothermal area in particular are well suited as analogs to potential Martian hydrothermal environments, certain key differences must be considered. Icelandic basalts are generally high in iron by terrestrial standards but still lower than many Martian basalts, including those from Gusev crater, and their Al concentrations tend to be higher than on Mars. Since the composition of the rock affects alteration pathways, basalt composition can affect the relative abundances and compositions of secondary minerals. Also, meteoric water plays a much larger role in Icelandic systems, and soluble salts and more mobile cations (e.g. Na, Ca, Mg) are more easily leached and removed from the system. However, while current conditions on Mars are drastically different from Earth, the atmospheric conditions on early Mars are far less constrained. The abundance of ferric minerals and phyllosilicates in Noachian terrains may indicate at least locally oxidizing conditions and/or abundant surface water that altered basaltic substrate. The gas chemistry is wholly unconstrained, but given the high levels of sulfur in Martian basalts, volcanism likely produced abundant volatiles in the form of SO_2 and/or H_2S gas (Gaillard et al., 2009).

Home Plate, Gusev Crater: Sulfate-rich Paso Robles class soils. Paso Robles class soils are among the most altered materials examined by the Spirit rover in Gusev crater, as demonstrated by high SO_3 concentrations (>31%) and abundant ferric sulfate minerals. Other phases identified were amorphous silica, Mg-sulfates, Ca-sulfates, Ca-phosphates, hematite, halite, and allophane (Ming et al., 2006; Yen et al., 2008). Yen et al. (2008) favored an alteration process in an acid-sulfate leaching environment (e.g. fumaroles or steam condensed into caustic pools) derived from magma degassing and/or oxidation alteration of crustal iron sulfide deposits. Hynek et al. (2013) argued that a fumarole origin was a good fit based on research on Cerro Negro

(Nicaragua) fumaroles. Home Plate, a remnant volcanic structure, indicates that high-temperature volcanic gases and fluids were once common in the area (Squyres et al., 2007; Schmidt et al., 2008). The localized nature of the Paso Robles soils at various elevations, including depressions and on slopes, accompanied by high S concentrations, further supports a fumarole origin (Schmidt et al., 2008, 2009). The presence of hydrated ferric sulfates indicates oxidizing, low pH conditions and, therefore, that these soils formed in a highly acidic environment (Bigham and Nordstrom, 2000).

Námafjall hot spring related deposits exhibit a diversity of sulfate minerals (see Table 1), along with sulfide minerals at depth, silica phases (both amorphous and crystalline), and clays. Most of the sulfates identified at Námafjall are iron-bearing, with some Ca-, Na-, Al-, and mixed cation varieties. Yen et al. (2008) noted greater abundances of Mg-sulfates in the Paso Robles soils, which constitute only a minor component of the soluble sulfate-salts at Námafjall, and could be absent entirely if halotrichite, rather than pickeringite, is the dominant member of the halotrichite group present. These differences may be attributed to variation in the major cations available in the parent rocks. Higher Mg contents in Martian basalts compared to Hverir and Námaskar∂ may have produced more Mg-sulfates during acid-sulfate alteration. Mg is also a highly mobile element under acid-sulfate conditions and the high solubility of Mg-sulfates is likely responsible for their low abundance, as they would be easily washed away during interaction with ground and surface water. Acid-sulfate alteration of Martian basalts may have been more akin to a closed-system, lacking abundant precipitation after formation, where Mg and other mobile elements would be retained in the products of alteration. Marcucci et al. (2013) discuss the high solubility of Mg-sulfates (and thus their low abundance) in terrestrial hydrothermal environments, suggesting that the presence and preservation of Mg-sulfates is an indicator of limited water interactions.

Paso Robles class soils also contain a mixture of poorly constrained ferric sulfates (Lane et al., 2008). In target Arad Samara, a Fe:S ratio of approximately 2:3 was obtained by the removal of hematite, silica, and Mg-sulfate from the bulk using elemental abundances. Ferrous sulfates are excluded from consideration because they are not consistent with the Spirit Mössbauer results. Parente et al. (2009) and Wang and Ling (2011) identified the ferric sulfate mineral ferricopiapite, based on a visible-near infrared (VIS-NIR) spectral variation (derived from Pancam spectra), attributed to dehydration after exposure to the Martian atmosphere. Ferricopiapite forms in low pH environments (pH <2.5) and under highly oxidizing conditions, typical of fumarolic settings (Wang and Ling, 2011). Other ferric sulfates are likely present, but cannot be easily constrained using available spectroscopic data. Other candidates include rhomboclase, paracoquimbite ($Fe^{3+}_2(SO_4)_3•9H_2O$), kornelite ($Fe^{3+}_2(SO_4)_3•7H_2O$), and yavapaiite ($KFe^{3+}(SO_4)_2$). Parente et al. (2009) also identified paracoquimbite in Paso Robles and Tyrone soils. Fe^{3+}-sulfates identified in the Námafjall area are ferricopiapite, rhomboclase, (natro)jarosite, and coquimbite, which is structurally homeotypic with paracoquimbite but contains some Al ($AlFe_3(SO_4)_6(H_2O)_{12} \cdot 6H_2O$). Pancam spectra eliminate jarosite as a viable option in the Paso Robles soils primarily because it lacks a convex upward shape at ~480 nm in VNIR spectra (Lane et al., 2008). The VNIR patterns of other ferric sulfates like ferricopiapite and rhomboclase exhibit this unusual spectral feature. At Námafjall, these minerals were identified in sulfur-rich fumarolic soils in low pH (~2) environments, similar to those interpreted for the salty sulfate soils at Tyrone and other sites in the Columbia Hills. The presence of these minerals in the sulfur-rich hot spring associated deposits of Námafjall supports the acid-sulfate fumarole model proposed by Yen et al. (2008). Alternatively, ferricopiapite may have formed from other sulfate phases through a combination of dehydration, neutralization, and oxidation (e.g. King & McSween, 2005; Lane et al. 2008), similar to pyrite oxidation and/or volcanic vapors observed at Námafjall.

Figure 8 presents a conceptual model for hot spring related alteration, with a focus on iron and sulfur bearing minerals. The parts of this system that are most mineralogically similar to the Paso Robles soils are the surface efflorescences most distant from the hot springs, and the surface and shallow sediments along the margin. This is because these areas show the highest degree of oxidation, in keeping with the Fe^{3+} sulfate phases observed in the Martian deposits. Ende and Szynkiewicz (2022) interpreted the absence of less oxidized phases like sulfides, elemental sulfur, and Fe^{2+} sulfates in the Gusev hydrothermal deposits compared to modern terrestrial hot spring environments (including at Námafjall) as evidence that they were oxidized later, likely after hydrothermal processes ceased.

Gale crater: hydrothermally-altered sedimentary rocks of Aeolis Mons. Hydrothermal processes have also been inferred for the formation of specific features at Gale crater. In particular, Yen et al. (2021) interpreted the observed occurrence of tridymite in the Murray Formation of Gale crater as being consistent with hydrothermal fluid interaction with sediments rather than volcanic deposition. The identification of cristobalite in hydrothermally-altered volcanic sediments in this study (and tridymite in other hot spring/fumarole environments, such as at Lassen, McHenry et al., 2017), could provide a terrestrial example of a hydrothermal, rather than high-temperature volcanic, origin for the Murray tridymite.

Implications

The alteration mineral assemblages and patterns of element enrichment and depletion are relevant to the interpretation of likely hydrothermal deposits on Mars, especially those observed by the Mars Exploration Rover (MER) Spirit in the Columbia Hills. Several key observations:

1) The presence of smectitic clays formed under acidic conditions in the vicinity of hot springs. Neutral to alkaline fluids are often invoked in models for early Mars to help explain widespread clay formation (in contrast to sulfate-rich deposits, attributed to later acidic conditions, e.g. Bibring et al., 2005). However, more recent geochemical modeling by Peretyazhko et al. (2018) is consistent with clay formation and stability under more acidic conditions.

2) The range of Fe^{3+} sulfate phases observed in the soils surrounding this acid-sulfate hot spring environment. Ferricopiapite, rhomboclase, and coquimbite are observed here and are candidates for the inferred Fe^{3+} sulfate phases in the Paso Robles soils investigated by MER Spirit at Gusev crater. The similarity in mineral assemblage suggests a common origin, though the presence of sulfides at Námafjall but not Paso Robles indicates more oxidizing conditions on Mars, either during formation or due to later alteration.

3) Most major cations are highly mobile in steam-derived acid-sulfate waters (pH <2.5) and were leached from the system, affecting bulk compositions and leading to a paucity of sulfate precipitates with Mg^{2+}, K^+, or Na^+. This contrasts with Martian sulfates, where Mg-sulfates are common. The wetter conditions in Iceland compared to early Mars likely contribute to this difference.

4) Pyrite oxidation and volcanic vapor condensation produce a series of Fe-and Al-sulfate-salts. Fe^{2+} sulfates are present closer to the acid fluid source, while Fe^{3+} sulfates dominate at greater distances and in surface samples, consistent with a redox gradient for both Fe and S. The redox gradients developed in the vicinity of the hot springs would provide the necessary redox couples and aqueous environment to support microbial metabolisms. Similar environments could have been present, and habitable, on early Mars (e.g. Grotzinger et al., 2014).

Together, these observations inform our interpretations of the environments under which fluid-rock interactions occurred on the surface of ancient Mars. Acid-sulfate fumarole or hot spring alteration is a plausible mechanism for the formation of some sulfate-rich soils on Mars (e.g., Paso Robles soils in the Columbia Hills), and smectitic clays can also form and be preserved in acid-sulfate environments (typically at the margins of activity).

Acknowledgments

The authors would like to thank Teri Gerard, Thomas McCollom, Ramy El-Maarry, and Sarah Black for their assistance in the field and Jordan Ludyan and Christopher Vickery for their help in the lab. This research was funded by grants from the UW-Milwaukee Research Growth Initiative (to McHenry) and NASA's Habitable Worlds (award NNX15AP15G to McHenry). Permission to export samples from Iceland was granted by the Icelandic Institute of Natural History.

Figures

Figure 1: Maps of (a) Iceland and the Krafla area, adapted from Gudmundsson and Arnorsson (2005), and (b and c) Námafjall geothermal field, with sampling sites from this study. Geologic map in (b) adapted from Saemundsson et al. (2012), satellite imagery in (c) from Google Earth.

Figure 2: Field photos of (a) the hot spring transect sampled at Hverir, (b) the runoff pool from a steam vent at Hverir from which fluid sample IV-14-4 was collected, and (c) the muddy hot spring at Hverir from which fluid sample IV-14-5 was collected.

Figure 3: Photos of the Hverir hot spring transect and XRD patterns for nearby surface samples. IV-14-1 indicates the position where the associated hot spring fluid sample was collected. IV-13-2 is a sample of the grey mud from the rim of the hot spring (71.5°C), and contains amorphous silica, anatase, sulfur, pyrite, and minor amounts of various sulfates (ferricopiapite, alunogen, jarosite, and natroalunite), indicating a range of oxidation states for both iron and sulfur. IV-13-3 is a white surface precipitate from the apron surrounding the mud pot (94.3°), and consists entirely of sulfates, including mostly halotrichite/pickeringite, with minor amounts of other Fe^{2+}

and Fe^{3+} sulfate phases. Sample IV-13-4, from orange surface sediment beyond the margins of the visible sulfate precipitate apron (43.7°C), contains mostly smectitic clay, rhomboclase, and amorphous silica, with minor phases including goethite, anatase, and kaolinite.

Figure 4: Photos of the site of the first Námaskar∂ hot spring and adjacent soil pit, with XRD patterns for select samples. Fluid sample IV-14-29 was collected from the murky hot spring indicated. Sample IV-17-7 is a white surface precipitate collected nearby, and consists entirely of sulfates (halotrichite/pickeringite, gypsum, and rozenite). Sample IV-14-31 is yellow-tan sediment from 6 cm depth in the pit (36.2°C), and contains mostly amorphous silica, anatase, and rhomboclase, with minor sulfur and natroalunite. Sample IV-14-30 is grey mud collected from the same pit at 10 cm depth (51.1°C), and contains amorphous silica, pyrite, and anatase with minor marcasite and kaolinite. The high background of this XRD pattern is attributable to iron fluorescence (this sample contains 11.69 wt% Fe_2O_3T).

Figure 5: Photos of the site of the second Námaskar∂ hot spring and adjacent soil pit, with XRD patterns for select samples. Fluid sample IV-14-23 was collected from the mud pot indicated. Sample IV-17-5 is grey mud from the rim of this hot spring, and consists of abundant kaolinite, anatase, sulfur, and pyrite with minor smectite. Sample IV-14-22 is a surface precipitate collected nearby, and consists almost exclusively of halotrichite/pickeringite (with trace gypsum and potentially tamarugite). Sample IV-14-24 is orange surface sediment from the top of the 2nd Námaskar∂ pit (34.1°C), and contains abundant smectitic clay and ferricopiapite, with minor amorphous silica, jarosite, and gypsum. Sample IV-14-26 is dark grey mud sampled at 8 cm depth in the pit (61.3°C), and contains abundant quartz and pyrite, with minor anatase, marcasite,

szomolnokite, and rhomboclase. High background in the XRD patterns from this site results from iron fluorescence, based on the abundance of Fe-bearing minerals and a 14.99 wt% Fe_2O_3T for sample IV-14-24.

Figure 6: x-y plots of element abundances for Hverir and Námaskar∂ hot spring-adjacent samples analyzed by XRF. The composition of the less altered hyaloclastite and lava samples are plotted in green in each plot for comparison. Plots A-D show concentrations of SiO_2, Fe_2O_3T, MgO, and Zr vs. TiO_2, respectively; plots E-G show concentrations of SiO_2, Al_2O_3, and K_2O vs. Fe_2O_3T, respectively. TiO_2 serves as a proxy for the degree of leaching and residual enrichment and shows a linear relationship with Zr (another relatively immobile element). SiO_2 is enriched in many samples, in general showing an inverse relationship to Fe_2O_3T. MgO and K_2O are lower in all samples compared to the substrate, consistent with their mobility during leaching.

Figure 7: Spider plot for the Námaskar∂ hill samples normalized against the least altered hyaloclastite substrate sample (IV-14-36). Missing data points indicate concentrations below the limits of detection. TiO_2 and Zr are concentrated in all samples, consistent with residual enrichment through leaching. SiO_2 is higher in most samples, also consistent with leaching.

Figure 8: Conceptual model for hot spring related alteration. Alteration apron is ~2 meters in diameter. Vertical blue bars represent oxidation-reduction boundaries between Fe^{2+}/Fe^{3+}, S^{2-}/SO_4^{2-}, and S_0/ SO_4^{2-} determined by surface mineralogy. X1 and X2 correspond to samples used for isocon plots in Figure 9. The oxidation front at depth is also indicated, with reducing conditions (and related mineral assemblages) below and more oxidizing conditions and

assemblages above, as observed in samples collected from pits. Sulfate minerals observed or inferred for the Paso Robles soils at Gusev crater are listed in bold. They are concentrated in the surface deposits and precipitates at greater distances from the hot spring, above the oxidation front, indicating more oxidizing conditions.

Figure 9: Isocon plots for two samples from the vicinity of a Hverir hot spring. Sample locations are marked as X1 and X2 on Figure 8. Enrichment and depletion of elements are assessed by their relation to the 1:1 ratio line. For these graphs, any element that plots above the line is enriched, below is depleted, and on the 1:1 ratio line is immobile relative to the fresher basalt (IV-13-15). (X1) In the orange precipitate/sediment, phosphorous, Fe, and siderophile elements (e.g. V and Cr) are enriched, while most major cations are depleted (IV-13-2). (X2) In the gray mud, all major cations are depleted with residually enriched Si, Ti, and Zr (IV-13-4). S is enriched in both samples.

Tables

Table 1: Hverir hot spring transect samples and XRD phases

Table 2: Námaskar∂ hot spring area samples and XRD phases

Online Materials Table 3: Hverir hot spring transect XRF major and trace elements

Online Materials Table 4: Námaskar∂ hot spring area XRF major and trace elements

Table 5: Hydrolab results (environmental parameters for sampled fluids)

Table 6: Ion concentrations for sampled fluids

References

Ármannsson, H. (1993). The geothermal system in Námafjall- Chemical compilation. Collaboration Project of Landsvikjunar and Orkustofnunar, OS-93053/JHD-29 B, 30p (in Icelandic).

Arnórsson, S. and Andrésdóttir, A. (1995) Processes controlling the distribution of boron and chlorine in natural waters in Iceland. *Geochimica et Cosmochimica Acta* 59:4125-4146.

Bibring, J.-P. et al. (2005), Mars surface diversity as revealed by the OMEGA/Mars Express observations. Science 307: 1576–1581.

Bigham, J.M., and Nordstrom, D.K. (2000). Iron and aluminum hydroxysulfates from acid sulfate waters. In: Alpers, C.N. et al., Eds. Sulfate Minerals. Reviews in Mineralogy and Geochemistry, V. 40, Mineralogical Society of America, Washington, D.C. pp. 351-403.

Black, S.R., Hynek, B.M., McHenry, L.J., McCollom, T.M., Cameron, B.I., Glenister, C. (*in revision*). Bulk mineralogy of surficial hydrothermal acid-sulfate deposits at Námafjall, Þeistareykir 1 Geothermal Field, and Hengill Volcano, Iceland: Implications for the identification and 2 interpretation of hydrothermal deposits on Mars. *Journal of Geophysical Research Planets.*

Byers, H., McHenry, L.J., and Grundl, T.J. (2016) Forty-nine major and trace element concentrations measured in Soil Reference Materials NIST SRM 2586, 2587, 2709a, 2710a and

2711a using ICP-MS and Wavelength Dispersive-XRF. *Geostandards and Geoanalytical Research* 40:433-445.

Carson, G.L., McHenry, L.J., Hynek, B.M., Cameron, B.I., Glenister, C., *revised, in review*. Mineralogy and bulk geochemistry of a fumarole at Hverir, Iceland: Analog for acid-sulfate leaching on Mars. Submitted to *American Mineralogist*.

El-Maarry M. R., Black S. R., Hynek B. M. and McHenry L. J. (2017) Mineralogy of Fumarolic Deposits from Iceland as Analogs for Ancient Hydrothermal Systems on Mars: Role of Temperature. In *Lunar and Planetary Science Conference*: 2870–2871.

Ende, J.J. and Szynkiewicz, A., 2021. Mechanisms of sulfate formation in acidic hydrothermal sites of Iceland, Lassen, Valles Caldera, and Yellowstone: Implications for possible oxidation pathways in martian volcanic settings. *Icarus*, *368*, p.114608.

Fernández-Remolar, D., Morris, R.V., Gruener, J.E., Amils, R., and Knoll, A.H. (2005) The Rio Tinto Basin, Spain: Mineralogy, sedimentary geobiology, and implications for interpretation of outcrop rocks at Meridiani Planum, Mars. *Earth and Planetary Science Letters* 240:149-167.

Fialips, C-I., Petit, S., Decarreau, A., and Beaufort, D. (2000) Influence of synthesis pH on kaolinite “crystallinity” and surface properties. *Clays and Clay Minerals* 48:173-184.

Gaillard, F., and Scaillet, B. (2009) The sulfur content of volcanic gases on Mars. *Earth and Planetary Science Letters* 279:34-43.

Geptner, A.R., Ivanovskaya, T.A., Pokrovskaya, E.V., Lyapunov, S.M., Savichev, A.T., Gorbunov, A.V., and Gor'kova, N.V. (2007) Hydrothermally altered hyaloclastites at the earth's surface in the rift zone of iceland; problem of the biochemogenic accumulation of trace elements. *Lithology and Mineral Resources* 42:453-476.

Grotzinger, J. P., Arvidson, R.E., Bell, J.F.III, Calvin, W., Clark, B.C., Fike, D.A., Golombek, M., Greeley, R., Haldemann, A., Herkenhoff, K.E., Jolliff, B.L., Knoll, A.H., Malin, M., McLennan, S.M., Parker, T., Soderblom, L., Sohl-Dickstein, J.N., Squyres, S.W., Sullivan, R., Tosca, N.J., and Watters, W.A. (2005) Stratigraphy and sedimentology of a dry to wet eolian depositional system, Burns formation, Meridiani Planum, Mars. *Earth and Planetary Science Letters* 240:11-72.

Gudmundsson, B.T., and Arnórsson, S. (2005) Secondary mineral-fluid equilibria in the Krafla and Námafjall geothermal systems, Iceland. *Applied Geochemistry* 20:1607-1625.

Hausrath, E.M., Golden, D.C., Morris, R.V., Agresti, D.G., and Ming, D.W. (2013) Acid sulfate alteration of fluorapatite, basaltic glass and olivine by hydrothermal vapors and fluids: Implications for fumarolic activity and secondary phosphate phases in sulfate-rich Paso Robles soil at Gusev Crater, Mars. *Journal of Geophysical Research* 118:1-13.

Heaney, P.J. (1994). Structure and chemistry of the low-pressure silica polymorphs. In: Heaney, P.J., Prewitt, C.T., Ginnes, G.V., Eds. Silica: Physical behavior, geochemistry, and materials applications. Reviews in Mineralogy V. 29. Mineralogical Society of America, Washington, D.C., 1-40.

Herdianita, N.R., Browne, P.R.L., Rodgers, K.A., and Campbell, K.A. (2000) Mineralogical and textural changes accompanying ageing of silica sinter. *Mineralium Deposita* 35:48-62.

Hynek, B.M., McCollom, T.M., Marcucci, E.C., Brugman, K., and Rogers, K.L. (2013). Assessment of environmental controls on acid-sulfate alteration at active volcanoes in Nicaragua: Applications to relic hydrothermal systems on Mars. *Journal of Geophysical Research: Planets* 118:2083-2104.

Hynek, B.M., Rogers, K.L., Antunovich, M., Avard, G., Alvarado, G.E. (2018). Lack of microbial diversity in extreme Mars analog settings: Poás volcano, Costa Rica, *Astrobiology* 18, DOI: 10.1089/ast.2017.1719.

Kaasalainen, H., & Stefansson, A. (2011). Sulfur speciation in natural hydrothermal waters, Iceland. *Geochimica et Cosmochimica Acta, 75*, 2777-2791.

Kaasalainen, H., and Stefánsson, A. (2012) The chemistry of trace elements in surface geothermal waters and steam, Iceland. *Chemical Geology* 330-331:60-85.

Kandori, K., Sakai, J., Ishikawa, T. (2000) Definitive effects of chloride ions on the formation of spherical hematite particles in a forced hydrolysis reaction. *Physical Chemistry Chemical Physics* 2:3293-3299.

King, P.L. and McSween, H.Y.Jr. (2005) Effects of H (sub 2) O, pH, and oxidation state on the stability of Fe minerals on Mars. *Journal of Geophysical Research* 110:E12S10.

Lane, M.D., Bishop, J.L., Dyar, M.D., King, P.L., Parente, M., and Hyde, B.C. (2008) Mineralogy of the Paso Robles soils on Mars. *American Mineralogist* 93:728-739.

Lynne, B.Y., Campbell, K.A., Perry, R.S., Browne, P.R.L., and Moore, J.N. (2006) Acceleration of sinter diagenesis in an active fumarole, Taupo volcanic zone, New Zealand. *Geology* 34:749-752.

Lynne, B.Y., Campbell, K.A., James, B.J., Browne, P.R.L., and Moore, J. (2007) Tracking crystallinity in siliceous hot-spring deposits. *American Journal of Science* 307:612-641.

Marcucci, E. C., B. M. Hynek, K. S. Kierein-Young, and K. L. Rogers, Visible to near-infrared spectroscopy of volcanic acid-sulfate weathering systems in Nicaragua: Analogs for early Mars alteration, *Journal of Geophysical Research - Planets*, 118, 2213–2233, doi:10.1002/jgre.20159, 2013.

Marcucci, E.C., Hynek, B.M. (2014). Laboratory simulations of acid-sulfate weathering under volcanic hydrothermal conditions: Implications for early Mars. *Journal of Geophysical Research Planets* 119:679-703.

Markússon, S.H., and Stefánsson, A. (2011) Geothermal surface alteration of basalts, Krýsuv k Iceland; alteration mineralogy, water chemistry and the effects of acid supply on the alteration process. *Journal of Volcanology and Geothermal Research* 206:46-59.

McCollom, T.M., and Hynek, B.M. (2005) A volcanic environment for bedrock diagenesis at Meridiani Planum on Mars. *Nature* 438:1129-1131.

McHenry, L.J., Carson, G.L., Dixon, D. T., Vickery, C.L. (2017). Secondary minerals associated with Lassen fumaroles and hot springs: Implications for martian hydrothermal deposits. *American Mineralogist* 102: 1418-1434. DOI: 10.2138/am-2017-5839

Ming, D.W., Mittlefehldt, D.W., Morris, R.V., Golden, D.C., Gellert, R., Yen, A., Clark, B.C., Squyres, S.W., Farrand, W.H., Ruff, S.W., Arvidson, R.E., Klingelhöfer, G., McSween, H.Y., Rodionov, D.S., Schröder, X., de Souza, P.A.Jr., and Want, A. (2006) Geochemical and mineralogical indicators for aqueous processes in the Columbia Hills of Gusev crater, mars. *Journal of Geophysical Research* 111:E02S12.

Mínguez, H.A., Ortega, L., Lunar, R., Martínez-Frías, J., and Piña, R. (2011) Mineralogy of the Hydrothermal Alteration in the Námafjall Geothermal Field (Iceland). *MACLA. Revista*

Española de la Sociedad de Mineralogia 15:25-26.

Morris, R.V., Golden, D.C., Bell III, J.F., Shelfer, T.D., Scheinost, A.C., Hinman, N.W., Furniss, G., Mertzman, S.A., Bishop, J.L., Ming, D.W. and Allen, C.C., 2000. Mineralogy, composition, and alteration of Mars Pathfinder rocks and soils: Evidence from multispectral, elemental, and magnetic data on terrestrial analogue, SNC meteorite, and Pathfinder samples. *Journal of Geophysical Research: Planets*, *105*(E1): 1757-1817.

Morris, R.V., Klingelhöfer, G., Schröder, C., Fleischer, I., Ming, D.W., Yen, A.S., Gellert, R., Arvidson, R.E., Rodionov, D.S., Crumpler, L.S., Clark, B.C., Cohen, B.A., McCoy, T.J., Mittlefehldt, D.W., Schmidt, M.E., de Souza, P.A.Jr., and Squyres, S.W. (2008) Iron mineralogy and aqueous alteration from Husband Hill through Home Plate at Gusev crater, Mars: Results from the Mös bauer instrument on the Spirit Mars Exploration Rover. *Journal of Geophysical Research* 113:E12S42.

Nordstrom, D.K., and Alpers, C.N. (1999) Geochemistry of acid mine waters. *Reviews in Economic Geology* 6A:133-160.

Peretyazhko, T., Sutter, B., and Ming, D.W. (2014) Alteration of basaltic glass to Mg/Fe smectite under acidic conditions: A potential smectite formation mechanisms on Mars. 51st Clay Minerals Society Meeting; 17-21 May 2014; College Station, TX; United States.

Peretyazhko, T.S., Niles, P.B., Sutter, B., Morris, R.V., Agresti, D.G., Le, L., and Ming, D.W. (2018). Smectite formation in the presence of sulfuric acid: Implications for acidic smectite formation on early Mars. *Geochimica et Cosmochimica Acta* 220: 248-260.

Reardon, E.J., and Beckie, R.D. (1987) Modelling chemical-equilibria of acid-mine drainage - the FeSO4-H2SO4-H2O system. *Geochimica et Cosmochimica Acta* 51:2355-2368.

Rodgers, K.A., Cook, K.L., Browne, P.R.L., and Campbell, K.A. (2002). The mineralogy, texture and significance of silica derived from alteration by steam condensate in three New Zealand geothermal fields. *Clay Minerals* 37:299–322.

Rodgers, K.A., Browne, P.R.L., Buddle, T.F., Cook, K.L., Greatrex, R.A., Hampton, W.A., Herdianita, N.R., Holland, G.R., Lynne, B.Y., Martin, R., Newton, Z., Pastars, D., Sannazarro, K.L., and Teece, C.I.A. (2004) Silica phases in sinters and residues from geothermal fields of New Zealand. *Earth Science Reviews* 66:1-61.

Ruff, S.W., Farmer, J.D., Calvin, W.M., Herkenhoff, K.E., Johnson, J.R., Morris, R.V., Rice, M.S., Arvidson, R.E., Bell, J.F. III, Christensen, P.R., and Squyres, S.W. (2011). Characteristics, distribution, origin, and significance of opaline silica observed by the Spirit rover in Gusev crater, Mars. *Journal of Geophysical Research* 116:E00F23.

Ruff, S.W., Campbell, K.A., Van Kranendonk, M., Rice, M.S., Farmer, J.D. (2020). The case for ancient hot springs in Gusev Crater, Mars. *Astrobiology* 20: 475-499.

Ruff, S.W., and Farmer, J.D. (2016). Silica deposits on Mars with features resembling hot spring biosignatures at El Tatio in Chile. *Nature Communications* 7:13554.

Saemundsson, K. (1991). The geology of the Krafla system. In: Nattura Myvatns, ed. Arnpor Gardarsson and Arni Einarsson. HIN, 24-95.

Saemundsson, K., Hjartarson, A., Kaldal, I., Sigurgeirsson, M.A., Kristinsson, S.G., and Vikingsson, S. (2012) Geological Map of the northern Volcanic Zone, Iceland. Northern Part. 1:100,000. Reykjavik: Iceland GeoSurvey and Landsvierkjun.

Schmidt, M.E., Ruff, S.W., McCoy, T.J., Farrand, W.H., Johnson, J.R., Gellert, R., ... and Schroeder, C. (2008). Hydrothermal origin of halogens at Home Plate, Gusev crater. *Journal of Geophysical Research: Planets*, 113(E6).

Schmidt, M.E., Farrand, W.H., Johnson, J.R., Schröder, C., Hurowitz, J.A., McCoy, T.J., ... and Ming, D.W. (2009). Spectral, mineralogical, and geochemical variations across Home Plate, Gusev Crater, Mars indicate high and low temperature alteration. *Earth and Planetary Science Letters* 281(3-4), 258-266.

Schulze-Makuch, D., Dohm, J.M., Fan, C., Fairén, A.G., Rodriguez, J.A.P., Baker, V.R., and Fink, W. (2007) Exploration of hydrothermal targets on Mars. *Icarus* 189:308-324.

Skok, J. R., Mustard, J. F., Ehlmann, B. L., Milliken, R. E., & Murchie, S. L. (2010). Silica deposits in the Nili Patera caldera on the Syrtis Major volcanic complex on Mars. *Nature Geoscience*, *3*(12), 838.

Squyres, S.W., Arvidson, R.E., Ruff, S., Gellert, R., Morris, R.V., Ming, D.W., Crumpler, L., Farmer, J.D., Des Marais, D.J., and Yen, A. (2008) Detection of silica-rich deposits on Mars. *Science* 320:1063–1067.

Squyres, S.W., Aharonson, O., Clark, B.C., Cohen, B.A., Crumpler, L., de Souza, P.A.J., Farrand, W.H., Gellert, R., Grant, J., Grotzinger, J.P., Haldemann, A.F.C., Johnson, J.R., Klingelhöfer, G., Lewis, K.W., Li, R., McCoy, T., McEwen, A.S., McSween, H.Y., Ming, D.W., Moore, J.M., Morris, R.V., Parker, T.J., Rice, J.W.Jr., Ruff, S.W., Schmidt, M., Schröder, C., Soderblom, L.A., and Yen, A. (2007). Pyroclastic activity at Home Plate in Gusev Crater, Mars. *Science* 316:738-742.

Stoiber, R.E., and Rose, W.I. (1974) Fumarole incrustations at active Central American volcanoes. *Geochimica et Cosmochimica Acta* 38:495-516.

Story, S., Bowen, B.B., Benison, K.C., and Schulze, D.G. (2010) Authigenic phyllosilicates in modern acid saline lake sediments and implications for Mars. *Journal of Geophysical Research* 115:E12012.

Tarnas, J.D., Mustard, J.F., Lin, H., Goudge, T.A., Amador, E.S., Bramble, M.S., Kremer, C.H., Zhang, X., Itoh, Y. and Parente, M., 2019. Orbital identification of hydrated silica in Jezero crater, Mars. *Geophysical Research Letters*, *46*(22), pp.12771-12782.

Velde, B. (Ed.) (1995). Origin and Mineralogy of Clays, Springs, New York.

Walter, M.R., and Des Marais, D.J. (1993). Preservation of biological information in thermal spring deposits: developing a strategy for the search for fossil life on Mars. *Icarus* 101:129-143.

Wang, A., Bell, J.F. III, Li, R., Johnson, J.R., Farrand, W.H., Cloutis, E.A., Arvidson, R.E., Crumpler, L., Squyres, S.W., and McLennan, S.M. (2008) Light-toned salty soils and coexisting Si-rich species discovered by the Mars Exploration Rover Spirit in Columbia Hills. *Journal of Geophysical Research* 113:E12S40.

Yen, A.S., Morris, R.V., Clark, B.C., Gellert, R., Knudson, A.T., Squyres, S., Mittlefehldt, D.W., Ming, D.W., Arvidson, R., McCoy, T., Schmidt, M., Hurowitz, J., Li, R., and Johnson, J.R. (2008) Hydrothermal processes at Gusev Crater: An evaluation of Paso Robles class soils. *Journal of Geophysical Research* 113:E06S10.

Yen, A.S., Morris, R.V., Ming, D.W., Schwenzer, S.P., Sutter, B., Vaniman, D.T., Treiman, A.H., Gellert, R., Achilles, C.N., Berger, J.A. and Blake, D.F., 2021. Formation of tridymite and evidence for a hydrothermal history at gale crater, Mars. *Journal of Geophysical Research: Planets*, *126*(3), p.e2020JE006569.

Zolotov, M.Y. and Shock, E.L. (2005). Formation of jarosite-bearing deposits through aqueous oxidation of pyrite at Meridiani Planum, Mars. *Geophysical Research Letters* 32:L21203.

Table 1: Hverir mudpot transect

						Non-sulfur bearing		Sulfur-bearing	
Sample	Type	Distance (cm)	Temp (°C)	pH	Description	Abundant	Minor	Abundant	Minor
IV-14-5	fluid	0	80.2	2.00	Bubbling muddy water on upthrown side of fault				
IV-13-2	sed	0	71.5		Dark mud at edge of mud pot	Si	Ka, At	S, Py	Fc, Ag, J, Na
IV-13-3	precip.	60	94.3		White/orange popcorn-like precipitate			HP, Gyp	Sz, Rh, V, Co, Rz
IV-13-4	sed	100	43.7		Red/orange sand	Sm, Gt	Si, Ka, At, Ct	Rh	
Other Hverir fluid samples									
IV-14-1	fluid	NA	40.9	2.12	Bubbling murky water on downthrown side of fault				
IV-14-4	fluid	NA	11.0	2.40	Pool of condensed steam from steam spout on upthrown side				
Hverir Holocene basalt substrate									
IV-13-15	rock				Unaltered substrate basalt	Pl, Aug			

Phases: Aug = augite, Ag = alunogen, At= anatase, Co= coquimbite, Ct = cristobalite, Fc = ferricopiapite, Gt = goethite, Gyp = gypsum, HP = halotrichite/pickeringite, J = jarosite, Ka = kaolinite, Na = natroalunite, Pl = plagioclase, Py = pyrite, Rh = rhomboclase, Rz = rozenite, S = sulfur, Si = amorphous silica, Sm = smectite, Sz = szomolnokite, V = voltaite.

Table 2: Námaskard hill sample details and XRD results

							Non-sulfur bearing		Sulfur-bearing	
Sample	Type	Distance (cm)	Depth (cm)	Temp (°C)	pH	Description	Abundant	Minor	Abundant	Minor
Námaskard hot spring #1										
IV-14-29	Fluid	0		70.5	2.3	Vigorous, more clear mud pot				
IV-17-07	precip.	nearby	0			White/light green fluffy precipitated minerals			Rz, HP, Gyp	
IV-14-31	sed	pit	6	36.2		Yellow/beige sed beneath surface crust	Si, At		Rh	S, Na
IV-14-32	sed	pit	10	51.1		Creamy, light grey sed	Si, At		S	Na, Fc
IV-14-30	sed	pit	28	75.2		Darker grey, softer sed	Si, At	Ka	Py	Mr
Námaskard hot spring #2										
IV-14-23	Fluid	0		56.4	2-2.3	Least muddy small mud pot				
IV-17-05	sed	0	0			Mud from rim of mud pot	Ka, At	Sm	S, Py	
IV-14-22	precip.	nearby	0			White, bulbous crystal precipitate			HP	Gyp, Ta
IV-14-24	sed	pit	0	34.1		Orange surface coating	Sm	Si	Fc	Gyp, J
IV-14-25	sed	pit	3	33.4		Light grey/beige sed	Q, At	Si		
IV-14-26	sed	pit	8	61.3		Dark grey sed	Q	At	Py	Mr, Sz, Rz

Phases: At= anatase, Fc = ferricopiapite, Gyp = gypsum, HP = halotrichite/pickeringite, J = jarosite, Ka = kaolinite, Mr = marcasite, Na = natroalunite, Py = pyrite, Q = quartz, Rh = rhomboclase, Rz = rozenite, S = sulfur, Si = amorphous silica, Sm = smectite, Sz = szomolnokite, Ta = tamarugite.

Table 5: *In-situ* Environmental parameters

Site	Sample	T°C	pH	SpCond (us/cm)	Sal (ppt)	ORP (mV)	TDS (g/l)
Hverir							
	IV-14-1	40	2.15	6163	3.41	-56	4.0
	IV-14-4	59	2.42	2109	1.13	-136	1.3
	IV-14-5	**66**	**2.20**	**4024**	**2.19**	**-343**	**2.7**
Námaskarð							
	IV-14-23	**56**	**2.24**	**4241**	**2.32**	**-269**	**2.7**
	IV-14-29	**71**	**2.36**	**1456**	**0.77**	**-302**	**0.9**

Bolded samples are for pools adjacent to reported transects.
SpCond: Specific conductivity. Sal: Salinity.
ORP: Oxidation/Reduction Potential. TDS: Total Dissolved Solids.

Table 6: Dissolved ions (mg/l)

Site	Sample	SiO_2	Na^+	K^+	Ca^{2+}	Mg^{2+}	Fe	Al*	Cl^-	SO_4^{2-}	NO_3^-
Hverir											
	IV-14-01	246	24.27	2.24	107.9	82.4	122	*425*	0.3	3819	8.7
	IV-14-04	197	63.37	6.23	90.9	19.4	14.6	*28*	1.82	872	3.69
	IV-14-05	**228**	**15.45**	**3.36**	**65.1**	**53.6**	**196**	***450***	**1.52**	**3801**	**8.83**
Námaskarð											
	IV-14-23	**232**	**6.92**	**0.33**	**85.3**	**40.1**	**149**	***194***	**0.28**	**2150**	**5.78**
	IV-14-29	**253**	**3.05**	**0.19**	**13.9**	**9.5**	**9.7**	***x***	**0.14**	**398**	**1.35**

*Al concentrations inferred based on charge balance.

Bolded samples are for pools adjacent to reported transects.

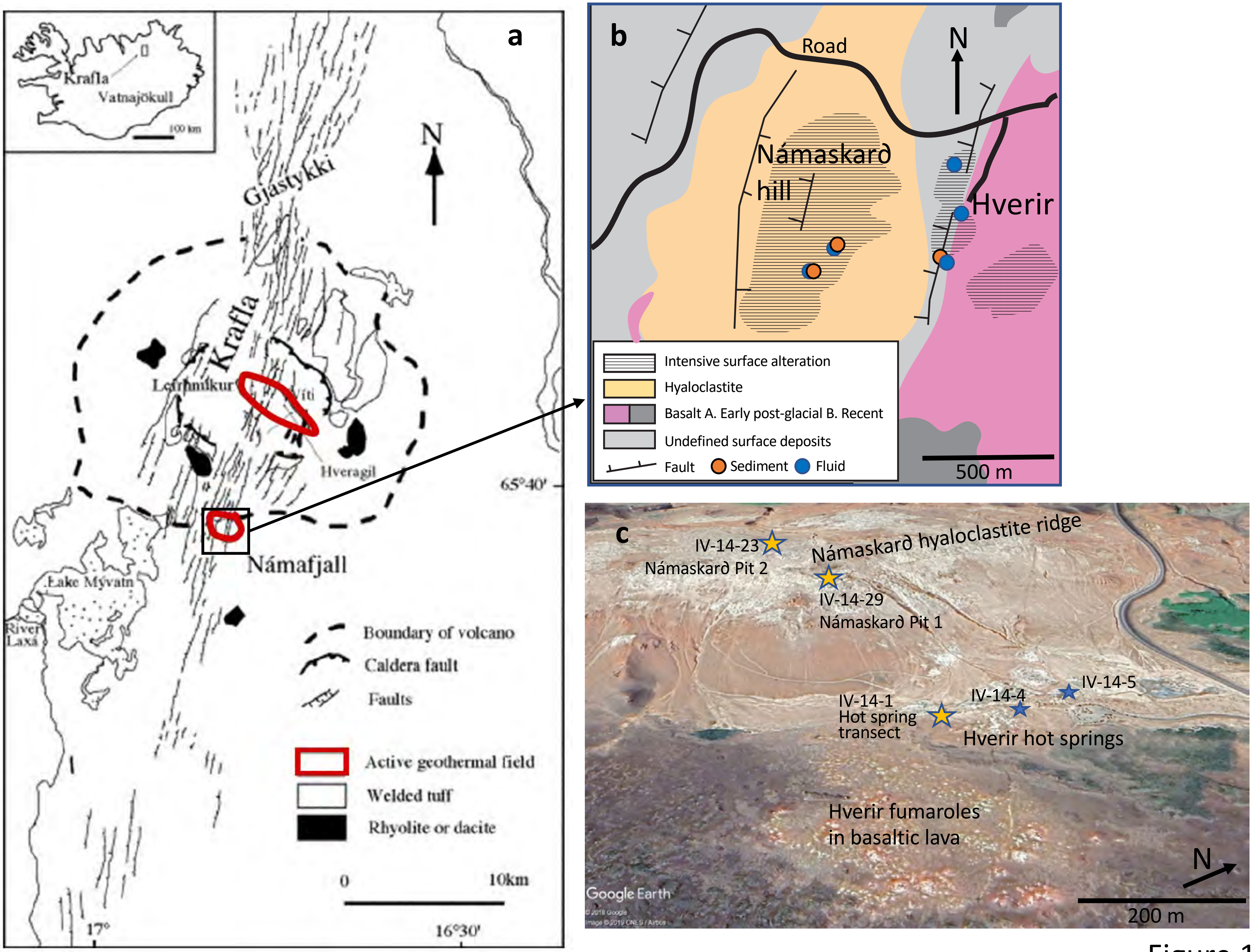
a
Krafla
Vatnajökull
100 km
N
Gjástykki
Krafla
Leirhnúkur
Víti
Hveragil
65°40'
Námafjall
Lake Mývatn
River Laxá
Boundary of volcano
Caldera fault
Faults
Active geothermal field
Welded tuff
Rhyolite or dacite
0
10km
17°
16°30'
b
Road
N
Námaskarð hill
Hverir
Intensive surface alteration
Hyaloclastite
Basalt A. Early post-glacial B. Recent
Undefined surface deposits
Fault
Sediment
Fluid
500 m
c
IV-14-23
Námaskarð Pit 2
Námaskarð hyaloclastite ridge
IV-14-29
Námaskarð Pit 1
IV-14-1
Hot spring transect
IV-14-4
IV-14-5
Hverir hot springs
Hverir fumaroles in basaltic lava
Google Earth
© 2018 Google
Image © 2019 CNES / Airbus
N
200 m

Figure 1

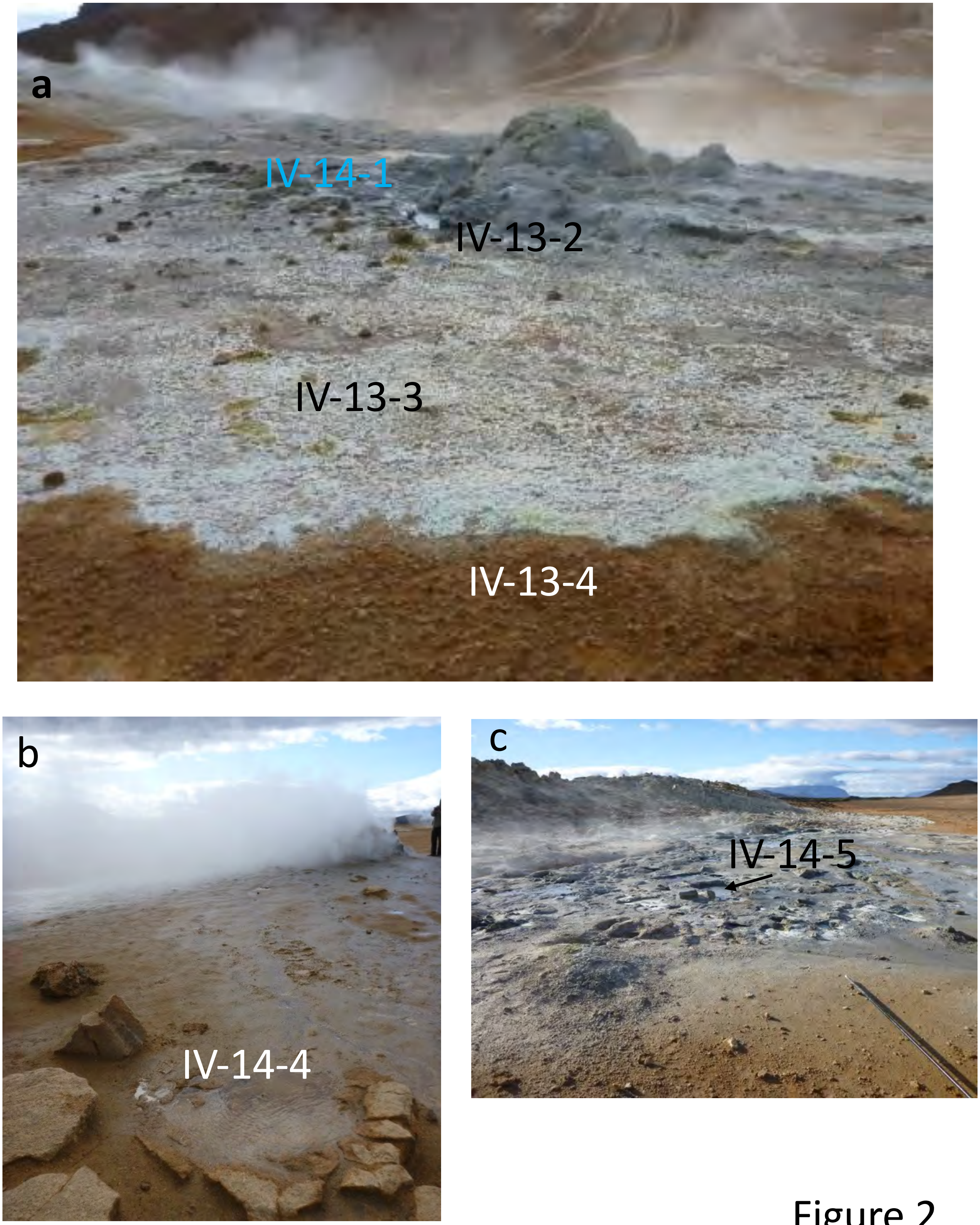

Figure 2

DOI: https://doi.org/10.2138/am-2022-8364. http://www.minsocam.org/

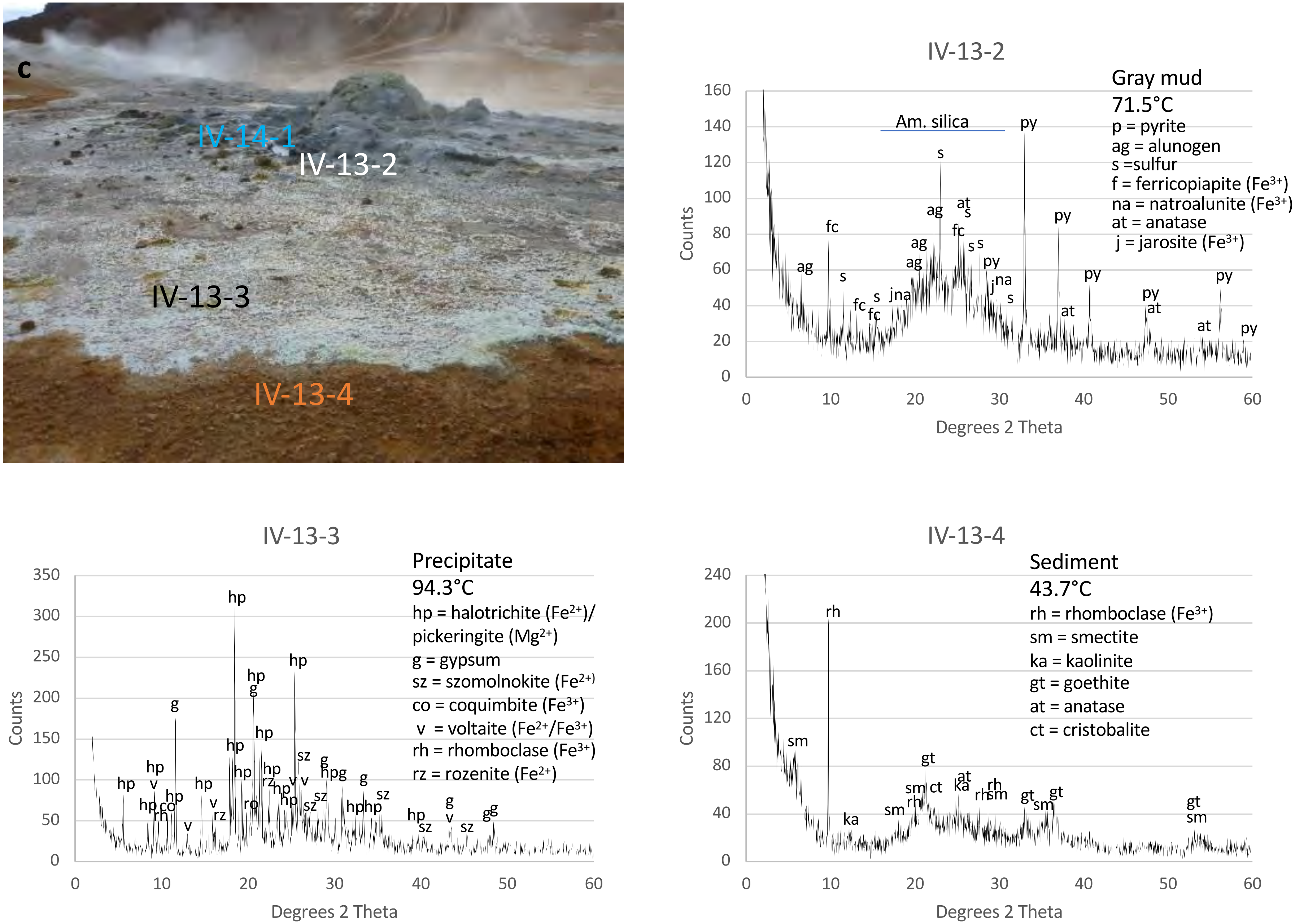

Figure 3

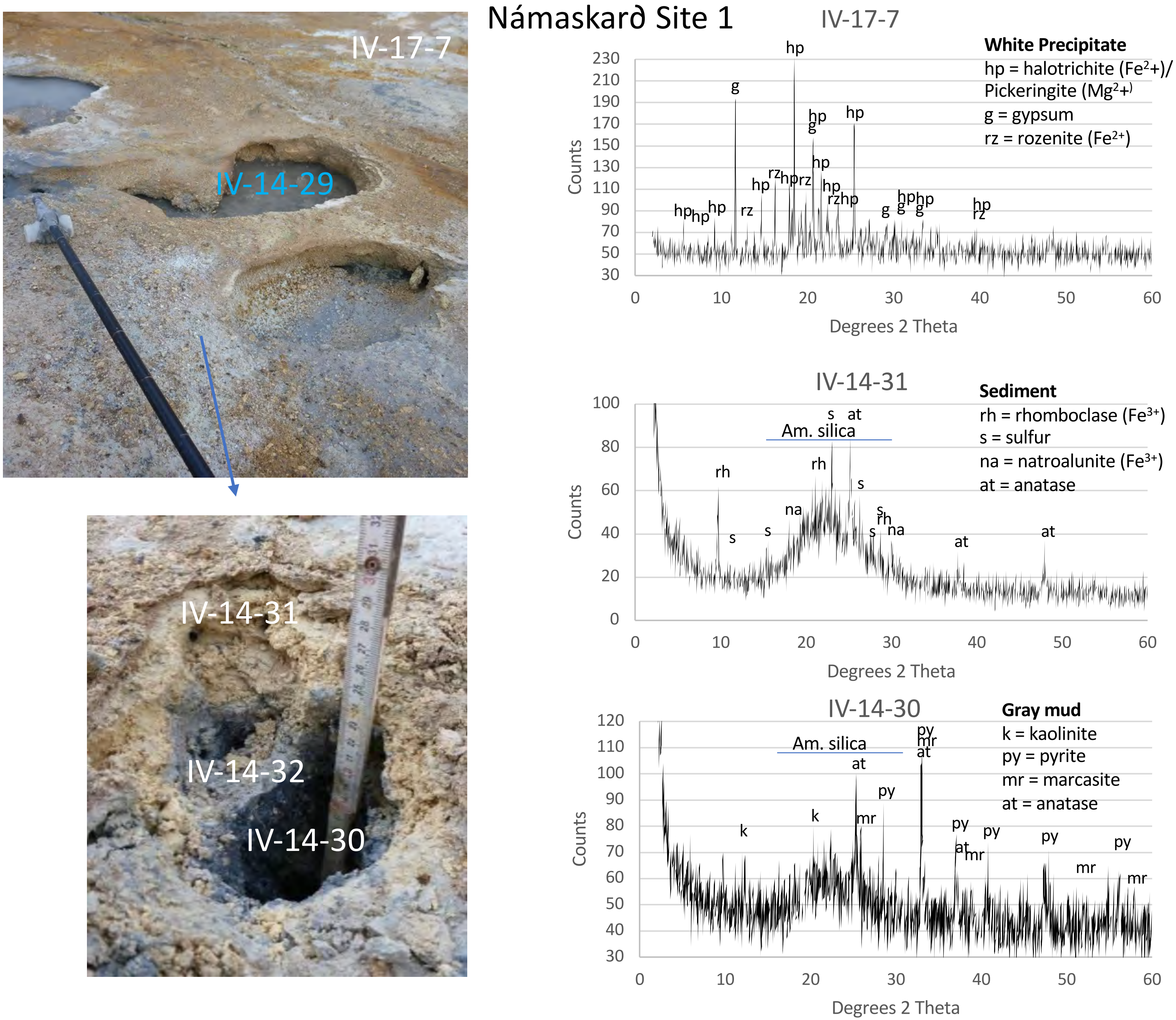
Námaskarð Site 1
IV-17-7
IV-14-29
IV-14-31
IV-14-32
IV-14-30
IV-17-7
White Precipitate
hp = halotrichite (Fe²+)/
Pickeringite (Mg²+)
g = gypsum
rz = rozenite (Fe²+)
Counts
Degrees 2 Theta
hp
g
hp
g
hp
hp
rz
hp
rz
hp
hp
hp
hp
hp
hp
rz
g
hp
g
hp
g
hp
rz
230
210
190
170
150
130
110
90
70
50
30
0
10
20
30
40
50
60
IV-14-31
Sediment
rh = rhomboclase (Fe³+)
s = sulfur
na = natroalunite (Fe³+)
at = anatase
Am. silica
s
at
rh
rh
s
na
s
s
rh
s
na
s
at
at
100
80
60
40
20
0
IV-14-30
Gray mud
k = kaolinite
py = pyrite
mr = marcasite
at = anatase
Am. silica
py
mr
at
at
py
k
mr
k
py
at
mr
py
py
mr
py
mr
120
110
100
90
80
70
60
50
40
30

Figure 4

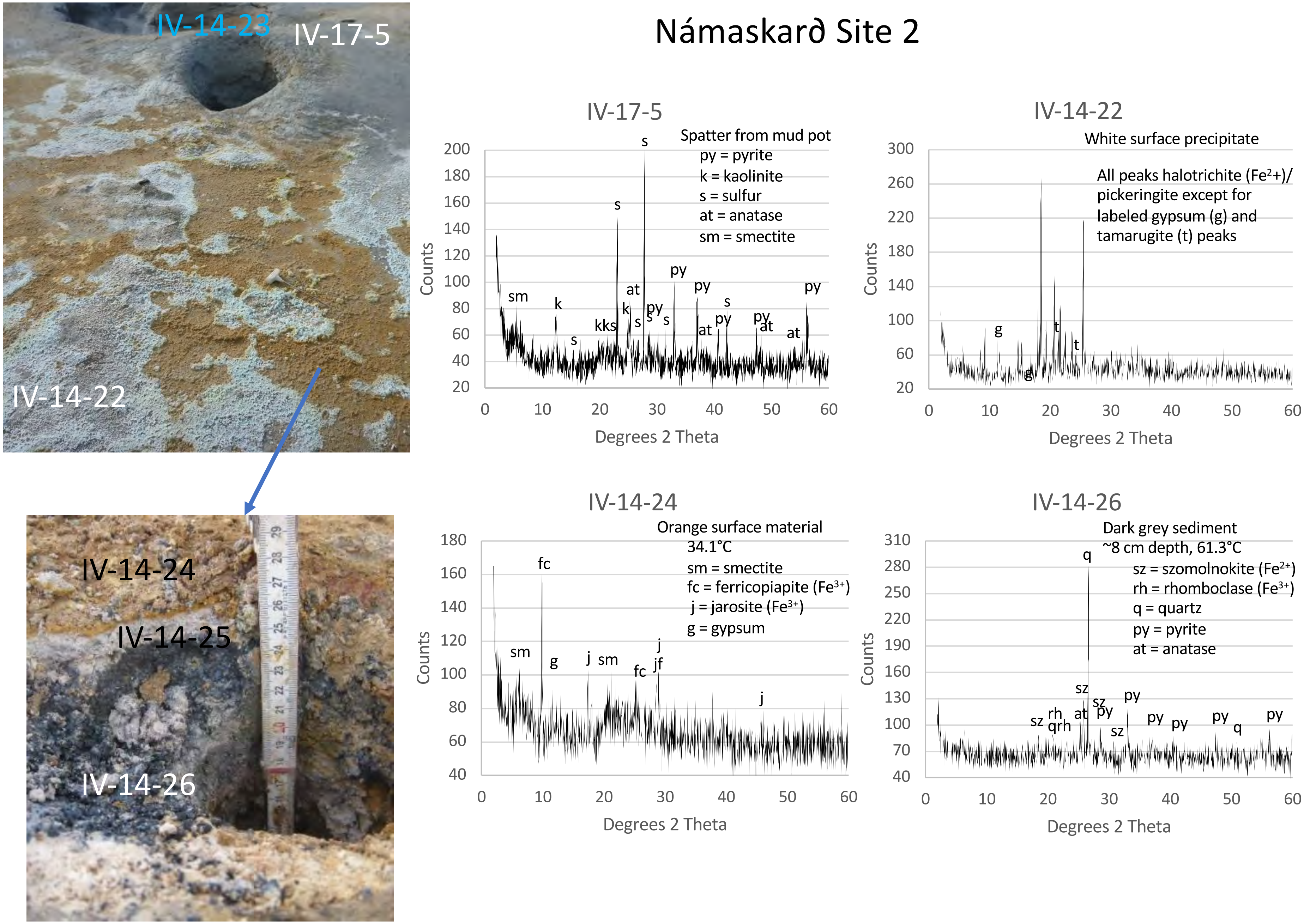
IV-14-23
IV-17-5
IV-14-22
IV-14-24
IV-14-25
IV-14-26
Námaskarð Site 2
IV-17-5
Spatter from mud pot
py = pyrite
k = kaolinite
s = sulfur
at = anatase
sm = smectite
Counts
Degrees 2 Theta
sm
k
s
kks
k
at
s
s
py
s
py
py
at
py
s
py
at
at
py
IV-14-22
White surface precipitate
All peaks halotrichite (Fe²+)/ pickeringite except for labeled gypsum (g) and tamarugite (t) peaks
g
g
t
t
IV-14-24
Orange surface material
34.1°C
sm = smectite
fc = ferricopiapite (Fe³⁺)
j = jarosite (Fe³⁺)
g = gypsum
sm
fc
g
j
sm
fc
j
jf
j
IV-14-26
Dark grey sediment
~8 cm depth, 61.3°C
sz = szomolnokite (Fe²⁺)
rh = rhomboclase (Fe³⁺)
q = quartz
py = pyrite
at = anatase
q
sz
sz
rh
qrh
at
sz
py
sz
py
py
py
py
q
py

Figure 5

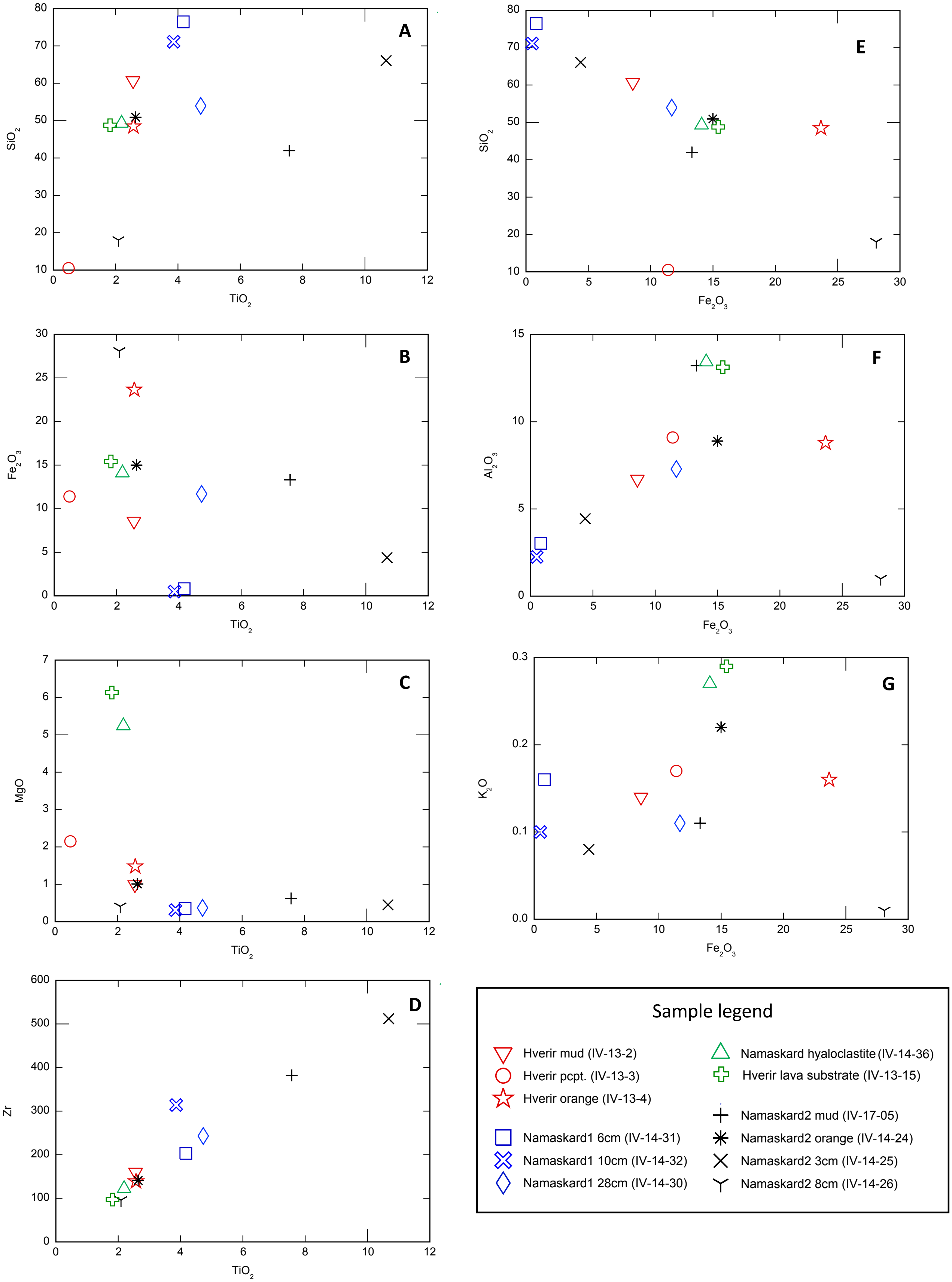
A
SiO2
TiO2
E
SiO2
Fe2O3
B
Fe2O3
TiO2
F
Al2O3
Fe2O3
C
MgO
TiO2
G
K2O
Fe2O3
D
Zr
TiO2
Sample legend
Hverir mud (IV-13-2)
Hverir pcpt. (IV-13-3)
Hverir orange (IV-13-4)
Namaskard1 6cm (IV-14-31)
Namaskard1 10cm (IV-14-32)
Namaskard1 28cm (IV-14-30)
Namaskard hyaloclastite (IV-14-36)
Hverir lava substrate (IV-13-15)
Namaskard2 mud (IV-17-05)
Namaskard2 orange (IV-14-24)
Namaskard2 3cm (IV-14-25)
Namaskard2 8cm (IV-14-26)

Figure 6

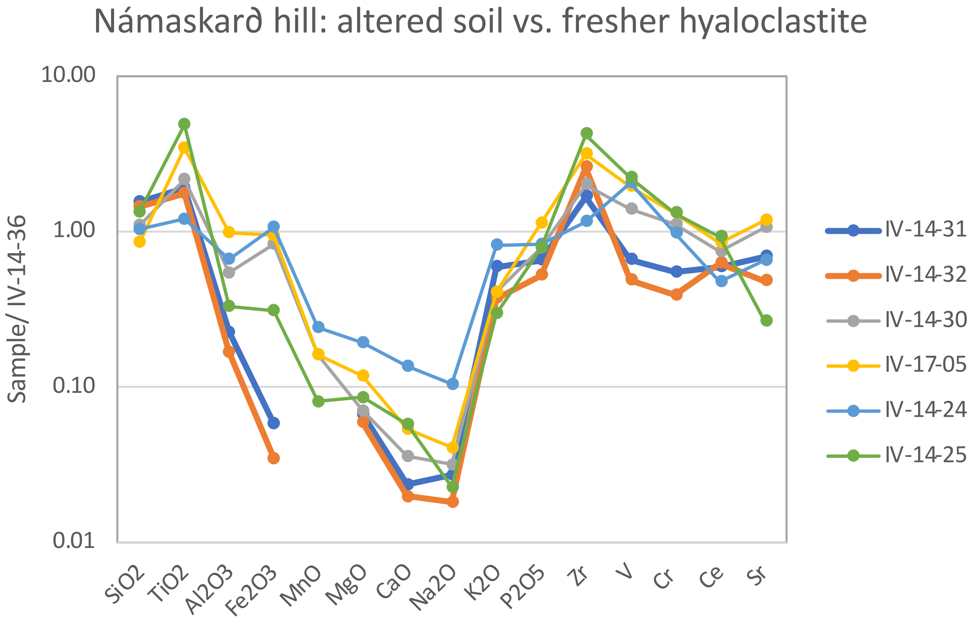
Námaskarð hill: altered soil vs. fresher hyaloclastite
10.00
1.00
0.10
0.01
Sample/ IV-14-36
SiO2
TiO2
Al2O3
Fe2O3
MnO
MgO
CaO
Na2O
K2O
P2O5
Zr
V
Cr
Ce
Sr
IV-14-31
IV-14-32
IV-14-30
IV-17-05
IV-14-24
IV-14-25

Figure 7

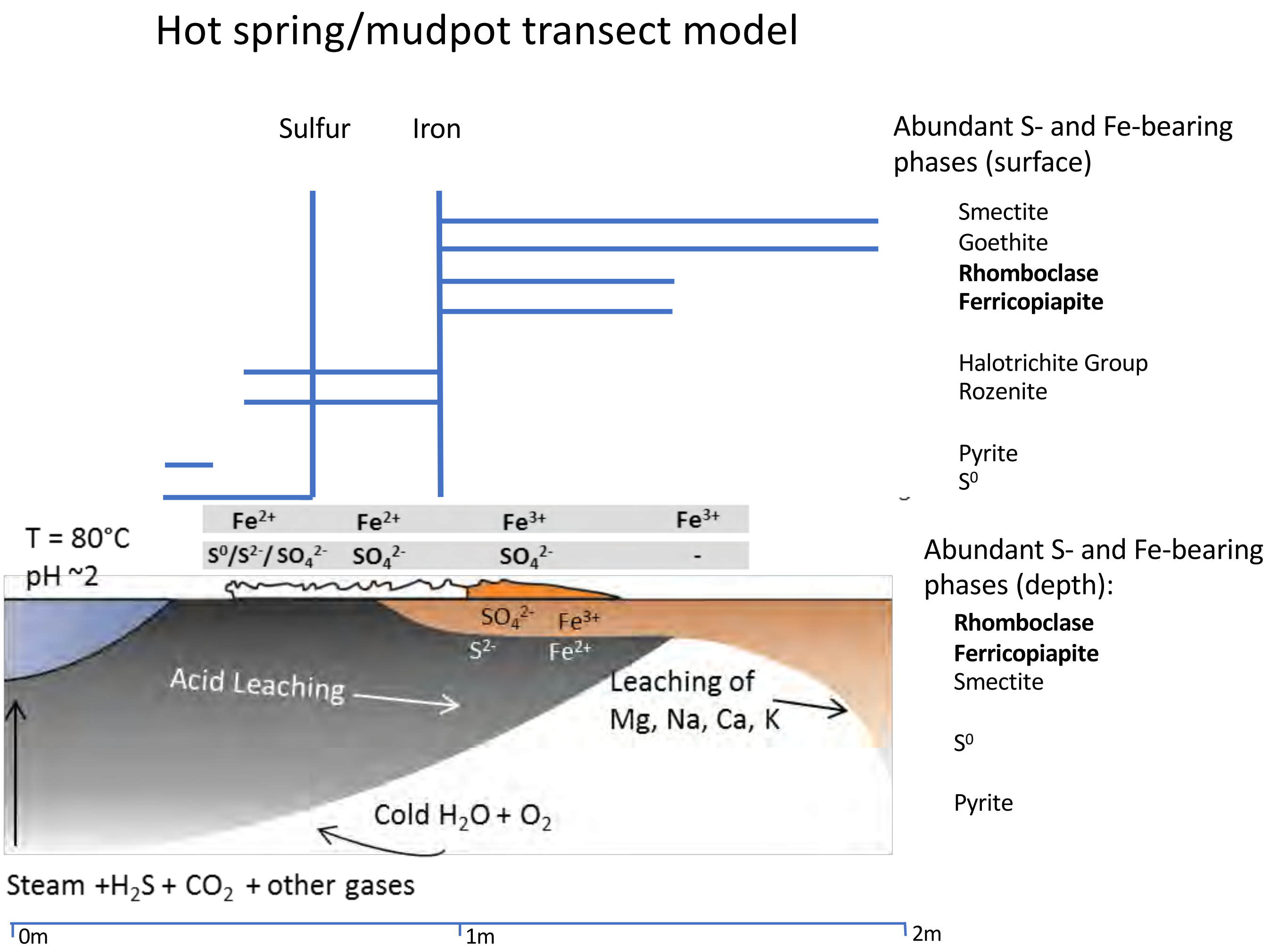
Hot spring/mudpot transect model
Sulfur
Iron
Abundant S- and Fe-bearing phases (surface)
Smectite
Goethite
Rhomboclase
Ferricopiapite
Halotrichite Group
Rozenite
Pyrite
S^0
T = 80°C
pH ~2
Fe^{2+}
Fe^{2+}
Fe^{3+}
Fe^{3+}
$S^0/S^{2-}/SO_4^{2-}$
SO_4^{2-}
SO_4^{2-}
-
SO_4^{2-}
Fe^{3+}
S^{2-}
Fe^{2+}
Acid Leaching
Leaching of Mg, Na, Ca, K
Cold $H_2O + O_2$
Steam $+H_2S + CO_2$ + other gases
Abundant S- and Fe-bearing phases (depth):
Rhomboclase
Ferricopiapite
Smectite
S^0
Pyrite
0m
1m
2m

Figure 8

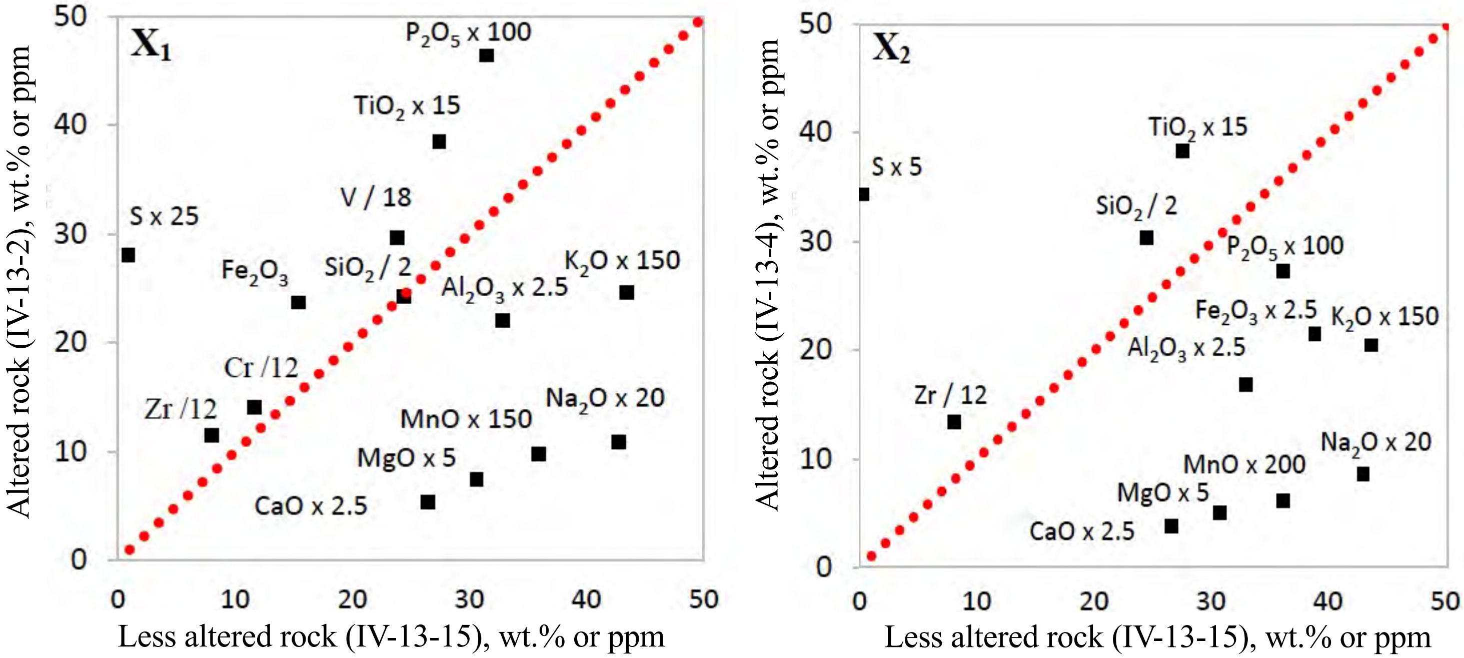
X1
Altered rock (IV-13-2), wt.% or ppm
Less altered rock (IV-13-15), wt.% or ppm
0
10
20
30
40
50
P2O5 x 100
TiO2 x 15
V / 18
S x 25
Fe2O3
SiO2 / 2
Al2O3 x 2.5
K2O x 150
Cr /12
Zr /12
Na2O x 20
MnO x 150
MgO x 5
CaO x 2.5
X2
Altered rock (IV-13-4), wt.% or ppm
Less altered rock (IV-13-15), wt.% or ppm
TiO2 x 15
S x 5
SiO2 / 2
P2O5 x 100
Fe2O3 x 2.5
K2O x 150
Al2O3 x 2.5
Zr / 12
Na2O x 20
MnO x 200
MgO x 5
CaO x 2.5

Figure 9